Estimation of vegetation canopy leaf area index and fraction of absorbed photosynthetically active radiation from atmosphere-corrected MISR data

Y. Knyazikhin,[1] J. V. Martonchik,[2] D. J. Diner,[2] R. B. Myneni,[1] M. Verstraete,[3] B. Pinty,[3] and N. Gobron[3]

Abstract. The multiangle imaging spectroradiometer (MISR) instrument is designed to provide global imagery at nine discrete viewing angles and four visible/near-infrared spectral bands. This paper describes an algorithm for the retrieval of leaf area index (LAI) and fraction of photosynthetically active radiation absorbed by vegetation (FPAR) from atmospherically corrected MISR data. The proposed algorithm is designed to utilize all the information provided by this instrument, using a two-step process. The first step involves a comparison of the retrieved spectral hemispherically integrated reflectances with those determined from the model which depend on biome type, canopy structure, and soil/understory reflectances. The biome/canopy/soil/understory models that pass this comparison test are subject to the second step, which is a comparison of their directional reflectances at the MISR angles to the retrieved spectral directional reflectances. This procedure, however, can produce multiple acceptable solutions. The measure theory is used to specify the most probable values of LAI and FPAR using the set of all acceptable solutions. Optimization of the retrieval technique for efficient global processing is discussed. This paper is the second of a two-part set describing a synergistic algorithm for producing global LAI and FPAR fields from canopy reflectance data provided by the MODIS (moderate resolution imaging spectroradiometer) and MISR instruments.

1. Introduction

The multiangle imaging spectroradiometer (MISR), an instrument onboard the EOS-AM1 platform, will make global observations of the Earth's surface at 1.1 km spatial resolution with the objective of determining the atmospherically corrected reflectance properties of most of the land surface and the tropical ocean [*Diner et. al.*, 1998a; *Martonchick et al.*, 1998]. Two types of atmospherically corrected bidirectional canopy reflectances and their integrated values will be available from this instrument. The hemispherical directional reflectance factor (HDRF) and bihemispherical reflectance (BHR) characterize surface reflectance under ambient sky conditions, i.e., direct and diffuse illumination. The HDRF and BHR are independent of the kind of canopy radiation model used and are shown to be highly accurate when correct atmospheric information is used [*Diner et al.*, 1998a, *Martonchick et al.*, 1998]. The bidirectional reflectance factor (BRF) and directional hemispherical reflectance (DHR) are defined for the special case when the atmosphere is absent. The removal of the effects of diffuse radiance from the HDRF requires the use of a model for the bidirectional reflectance distribution function (BRDF) which makes the retrieved BRF and DHR model dependent. The accuracy of these variables is lower than that for the HDRF and BHR because they include uncertainties in BRDF models. However, the BRF in the visible spectral bands allows for better characterization of the angular signature of canopy reflectances because it does not depend on atmospheric conditions, i.e., the BRFs have more intrinsic canopy information. Therefore a technique for the interpretation of these data must account for these features of retrieved canopy reflectances. The aim of this paper is to derive an algorithm for the retrieval of leaf area index (LAI) and fraction of photosynthetically active radiation absorbed by vegetation (FPAR) from canopy reflectances satisfying these requirements.

The measure theory is used to establish relationships between the surface reflectances, uncertainties in their retrieval, and canopy structure. This technique is a powerful way to relate values one quantifies (e.g., probabilities, weights, mass, volume, area, etc.) to the information one measures. Directly or indirectly, most modern approaches use measures. Therefore we use this technique to make the algorithm flexible, i.e, to incorporate various approaches within one algorithm. The measure theory starts with a description of spaces of all possible situations encountered in reality and which are taken into account by the retrieval technique. Therefore the second section begins with a

[1]Department of Geography, Boston University, Massachusetts.
[2]Jet Propulsion Laboratory, California Institute of Technology, California.
[3]Space Application Institute of the EC Joint Research Center, Italy.

description of the spaces of canopy realizations and observations of canopy reflectances, as well as the establishment of relationships between these spaces and uncertainties in measured canopy reflectances. The proposed algorithm aims to retrieve the most probable values of LAI and FPAR using these relationships. Numerical examples demonstrate the retrieval capability of this approach. In section 3, we analyze the case when canopy reflectances are only slightly sensitive to the canopy realizations and how this situation can be quantified. Some basic information on measure theory is presented in the Appendix. The algorithm interacts only with elements of the spaces of canopy realizations and observations of canopy reflectances. These spaces are static element of the algorithm, i.e., look-up table termed the CART (canopy architecture radiative transfer) file in the MISR Algorithm Theoretical Basis Document [*Diner et al.*, 1998b]. This provides the independence of the algorithm from a particular canopy radiation model. A question then arises as to how the CART file has to be filled in. In answering this question, we aimed (1) to minimize the size of the CART file and (2) to minimize the dependence of the CART file on a particular canopy radiation model. These problems are discussed in sections 4 through 8. Evaluation of FPAR is presented in section 9. Section 10 summarizes the flow of the MISR LAI/FPAR algorithm.

An Algorithm Theoretical Basis Document (ATBD) for the MISR surface retrieval algorithm is available at http://www-misr.jpl.nasa.gov and includes implementation details of the LAI/FPAR retrieval technique. This paper presents a theoretical exposition of the LAI/FPAR algorithm that will be implemented at launch.

2. Description of LAI Retrieval

Let $r_\lambda(\Omega,\Omega_0)$ and $A_\lambda^{\text{hem}}(\Omega_0)$ be the atmospherically corrected hemispherical directional reflectance factor (HDRF) and bihemispherical reflectance (BHR). We follow the definitions given by *Diner et al.* [1998a], which are also used in section 4. Note that both of these variables depend on the wavelength λ and the direction Ω_0 of direct solar radiance, soil reflectance properties, and incident (direct and diffuse) radiance. The HDRF also depends on view direction Ω. In order to quantify a proportion between the direct and the diffuse components of the incoming radiation, we use the ratio f_{dir} of direct radiation to the total (direct and diffuse) radiation incident on the canopy. If $f_{\text{dir}}=1$, the HDRF and BHR become the bidirectional reflectance factor (BRF) and directional hemispherical reflectance (DHR), respectively. Therefore the symbols $r_\lambda(\Omega,\Omega_0)$ and $A_\lambda^{\text{hem}}(\Omega_0)$ will denote, depending on the value of f_{dir}, the HDRF and BHR or the BRF and DHR. For each pixel the MISR instrument provides the atmospherically corrected HDRF, BHR, BRF, and DHR in nine view directions and at four spectral bands [*Diner et al.*, 1998a]. This information is the input to our LAI/FPAR retrieval algorithm which we express in the vector-matrix form as

$$\bar{r}(\Omega_0) = \begin{pmatrix} r_{\lambda_1}(\Omega_1,\Omega_0) & r_{\lambda_2}(\Omega_1,\Omega_0) & r_{\lambda_3}(\Omega_1,\Omega_0) & r_{\lambda_4}(\Omega_1,\Omega_0) \\ r_{\lambda_1}(\Omega_2,\Omega_0) & r_{\lambda_2}(\Omega_2,\Omega_0) & r_{\lambda_3}(\Omega_2,\Omega_0) & r_{\lambda_4}(\Omega_2,\Omega_0) \\ \vdots & \vdots & \vdots & \vdots \\ r_{\lambda_1}(\Omega_9,\Omega_0) & r_{\lambda_2}(\Omega_9,\Omega_0) & r_{\lambda_3}(\Omega_9,\Omega_0) & r_{\lambda_4}(\Omega_9,\Omega_0) \end{pmatrix},$$

(1)

$$\vec{A}^{\text{hem}}(\Omega_0) = [A_{\lambda_1}^{\text{hem}}(\Omega_0) \ A_{\lambda_2}^{\text{hem}}(\Omega_0) \ A_{\lambda_3}^{\text{hem}}(\Omega_0) \ A_{\lambda_4}^{\text{hem}}(\Omega_0)].$$

(2)

Here λ_1=446 nm, λ_2=558 nm, λ_3=672 nm, and λ_4=866 nm are the centers of the MISR spectral bands; Ω_i, i=1, 2, … , 9 are unit view direction vectors. We will use $r_\lambda(\Omega,\Omega_0)$, $A_\lambda^{\text{hem}}(\Omega_0)$, $\bar{r}(\Omega_0)$, and $\vec{A}^{\text{hem}}(\Omega_0)$ to denote modeled canopy reflectances and $\tilde{r}_\lambda(\Omega,\Omega_0)$, $\tilde{A}_\lambda^{\text{hem}}(\Omega_0)$, $\tilde{\bar{r}}(\Omega_0)$, and $\tilde{\vec{A}}^{\text{hem}}(\Omega_0)$ to denote observations of these variables.

The modeled canopy reflectances depend on the model parameters. In our algorithm we use a vegetation land cover classification parameterized in terms of variables used in photon transport theory [*Myneni et al.*, 1997]. It distinguishes six biome types, each representing a pattern of the architecture of an individual tree (leaf normal orientation; stem-trunk-branch area fractions; leaf and crown size) and the entire canopy (trunk distribution, topography), as well as patterns of spectral reflectance and transmittance of vegetation elements. The soil and/or understory type are also characteristics of the biome which can vary continuously within given biome-dependent ranges. The distribution of leaves is described by the three-dimensional leaf area density distribution function which can also depend on some continuous parameters (section 5). Therefore LAI may not be in the list p of model parameters directly. However, LAI can be obtained when model parameter values in the parameter list p are known; that is, LAI is a function of p: LAI=$l(p)$. The function l is assumed known. Thus the model parameter list p contains one discrete variable (biome type) which can take on six values only, continuous variables (the soil and/or understory type), and some continuous parameters determining the leaf area density distribution function. A detailed description of canopy parameterization is presented by *Knyazikhin et al.* [this issue]. The model parameters are said to be a canopy realization if values of model variables in the parameter list are specified. We denote by P a set of all possible canopy realizations and will use p to denote a canopy realization. The set P is the sum of six subsets,

$$P = \bigcup_{\text{bio}=1}^{6} P_{\text{bio}},$$

each representing a biome specific set of canopy realizations. Let $D_r \subset R^{4\times9}$ and $D_A \subset R^4$ be the space of all possible values of canopy reflectances obtained by running p over the set P; that is,

$$D_A = \left\{ \vec{A}^{\text{hem}}(\Omega_0,p) : p \in P \right\}, \quad D_r = \left\{ \bar{r}(\Omega_0,p) : p \in P \right\}. \quad (3)$$

Here we proceed with the suggestion that the sets D_A and D_r represent all possible observations of canopy reflectances; that is, any $\vec{\tilde{A}}^{\,\mathrm{hem}}(\Omega_0)$ and $\overline{\tilde{r}}(\Omega_0)$ are elements of D_A and D_r, respectively. It should be noted, however, that this suggestion may be violated in real situations.

In reality any model can simulate a process to within a certain degree of accuracy only. Also, measurements cannot be carried out ideally. It means that the models predict domains $O_A \subset D_A$ and $O_r \subset D_r$ around $\vec{A}^{\,\mathrm{hem}}(\Omega_0)$ and $\overline{r}(\Omega_0)$ to which the "true values" belong. The same is valid for measured quantities; that is, we can only point out neighborhoods O_A and O_r around $\vec{\tilde{A}}^{\,\mathrm{hem}}(\Omega_0)$ and $\overline{\tilde{r}}(\Omega_0)$ to which the "true values" belong. The domains O_A and O_r are uncertainties in measurements and simulations: any element from these domains can be true values. We define neighborhoods O_A and O_r about measured reflectances $\vec{\tilde{A}}^{\,\mathrm{hem}}(\Omega_0)$ and $\overline{\tilde{r}}(\Omega_0)$ as [*Diner et al.*, 1998a]

$$O_A = \left\{ \vec{A}^{\,\mathrm{hem}}(\Omega_0) \in D_A : \Delta_A\!\left[\vec{A}^{\,\mathrm{hem}}(\Omega_0), \vec{\tilde{A}}^{\,\mathrm{hem}}_\lambda(\Omega_0) \right] \le h_A \right\},$$
(4)

$$O_r = \left\{ \overline{r}(\Omega_0) \in D_r : \Delta_r[\overline{r}(\Omega_0), \overline{\tilde{r}}(\Omega_0)] \le h_r \right\},$$

where

$$\Delta_A\!\left[\vec{A}^{\,\mathrm{hem}}(\Omega_0), \vec{\tilde{A}}^{\,\mathrm{hem}}(\Omega_0) \right]$$
$$= \frac{\displaystyle\sum_{l=1}^{4} \nu_A(l)\left[\dfrac{A^{\mathrm{hem}}_{\lambda_l}(\Omega_0) - \tilde{A}^{\mathrm{hem}}_{\lambda_l}(\Omega_0)}{\sigma_A(l)} \right]^2}{\displaystyle\sum_{l=1}^{4} \nu_A(l)},$$
(5)

$$\Delta_r\!\left[\overline{r}(\Omega_0), \overline{\tilde{r}}(\Omega_0) \right]$$
$$= \frac{\displaystyle\sum_{l=1}^{4}\sum_{j=1}^{9} \nu_r(l,j)\cdot\left[\dfrac{r_{\lambda_l}(\Omega_j,\Omega_0) - \tilde{r}_{\lambda_l}(\Omega_j,\Omega_0)}{\sigma_r(l,j)} \right]^2}{\displaystyle\sum_{i=1}^{4}\sum_{j=1}^{9} \nu_r(l,j)}.$$

Here $\nu_A(l)=1$ if the BHR (or DHR) at wavelength λ_l exists and 0 otherwise; $\nu_r(l,j)$ takes on the value 1 if the HDRF (or BRF) at wavelength λ_l and in scattering direction Ω_j exists and 0 otherwise; σ_A and σ_r are uncertainties in the BHR (or DHR) and HDRF (or BRF) retrievals and h_r and h_A some configurable threshold values [*Diner et al*, 1998a]. Thus modeled quantities are defined to belong to a neighborhood around the measured values such that a model which differs from the retrieved BHR (or DHR) and HDRF (or BRF) values by an amount equivalent to or less than the retrieval uncertainty will result in values Δ_A and Δ_r of the order of unity.

Any canopy realization $p \in P$ for which $\overline{r}(\Omega_0) \in O_r$ and $\vec{A}^{\,\mathrm{hem}}(\Omega_0) \in O_A$ must be considered a candidate for a true p. Let us introduce sets of candidates for the solution as follows:

$$Q_A(L,O_A;P_{\mathrm{bio}}) = \left\{ p \in P_{\mathrm{bio}} : l(p) < L \text{ and } \vec{A}^{\,\mathrm{hem}}(\Omega_0) \in O_A \right\},$$

$$Q_r(L,O_r;P_{\mathrm{bio}}) = \left\{ p \in P_{\mathrm{bio}} : l(p) < L \text{ and } \overline{r}(\Omega_0) \in O_r \right\}.$$

These sets are subsets of P_{bio} and contain such p from P_{bio} for which the leaf area index LAI=$l(p)$ is less than a given value L from the interval [LAI$_{\mathrm{min}}$(bio), LAI$_{\mathrm{max}}$(bio)] and $\overline{r}(\Omega_0) \in O_r$, $\vec{A}^{\,\mathrm{hem}}(\Omega_0) \in O_A$. Here

$$\mathrm{LAI}_{\mathrm{min}}(\mathrm{bio}) = \inf\left\{ l(p) : p \in P_{\mathrm{bio}} \right\},$$

$$\mathrm{LAI}_{\mathrm{max}}(\mathrm{bio}) = \sup\left\{ l(p) : p \in P_{\mathrm{bio}} \right\}.$$

The sets $Q_A(\mathrm{LAI}_{\mathrm{max}},O_A;P_{\mathrm{bio}})$ and $Q_r(\mathrm{LAI}_{\mathrm{max}},O_r;P_{\mathrm{bio}})$ contain all $p \in P_{\mathrm{bio}}$ for which a canopy radiation model generates output comparable with measured data. In terms of these notations we formulate the inverse problem as follows: given atmospherically corrected canopy reflectances $\vec{\tilde{A}}^{\,\mathrm{hem}}(\Omega_0)$, $\overline{\tilde{r}}(\Omega_0)$ and their uncertainties O_A, O_r find all $p \in P_{\mathrm{bio}}$ for which

$$\vec{A}^{\,\mathrm{hem}}(\Omega_0) \in O_A \ ,$$
(6)

$$\overline{r}(\Omega_0) \in O_r \ .$$
(7)

The algorithm is designed to utilize all the available information of the observations by means of a two-step process. The first step involves a comparison of the retrieved spectral hemispherically integrated reflectances with those evaluated from the model, i.e., solution of (6). Only those p which satisfy this test are subject to the second step, which is a comparison of their directional reflectances at the MISR angles to the retrieved spectral directional reflectances, i.e.,the solution of (7).

In order to quantify solutions of (6) and (7) we introduce measures (distribution functions) defined on the set P_{bio} as follows: The subset P_{bio} is represented as a sum of nonintersected subsets

$$P_{\mathrm{bio}} = \bigcup_{k=1}^{N} P_{\mathrm{bio},k}, \quad P_{\mathrm{bio},k} \cap P_{\mathrm{bio},j} = \varnothing, \quad k \ne j \ .$$
(8)

Let $N_A(L;P_{\mathrm{bio}})$ and $N_{r,A}(L;P_{\mathrm{bio}})$ be numbers of subsets $P_{\mathrm{bio},k}$ containing at least one element from the set $Q_A(L,O_A;P_{\mathrm{bio}})$ and $Q_{A,r}(L)=Q_A(L,O_A;P_{\mathrm{bio}}) \cap Q_r(L,O_r;P_{\mathrm{bio}})$, respectively. As measures of $Q_A(L,O_A;P_{\mathrm{bio}})$ and $Q_{r,A}(L)$, we introduce biome-specific functions $F_{A,\mathrm{bio}}(L)$ and $F_{r,A,\mathrm{bio}}(L)$ as

$$F_{A,\mathrm{bio}}(L) = \lim_{N\to\infty} \frac{N_A(L;P_{\mathrm{bio}})}{N_A(\mathrm{LAI}_{\mathrm{max}};P_{\mathrm{bio}})} \ ,$$
(9)

$$F_{r,A,\mathrm{bio}}(L) = \lim_{N\to\infty} \frac{N_{r,A}(L;P_{\mathrm{bio}})}{N_{r,A}(\mathrm{LAI}_{\mathrm{max}};P_{\mathrm{bio}})} \ .$$
(10)

A mathematical description of the convergence process is presented in the Appendix. Intuitively, the subset $P_{\mathrm{bio},k}$ specifies a set of canopy realizations whose range of variation is "sufficiently small." $N_A(\mathrm{LAI}_{\mathrm{max}};P_{\mathrm{bio}})$ and $N_{r,A}(\mathrm{LAI}_{\mathrm{max}};P_{\mathrm{bio}})$ are total number of solutions of (6) and (7); $N_A(L;P_{\mathrm{bio}})$ and $N_{r,A}(L;P_{\mathrm{bio}})$ are the number of these solutions when LAI=$l(p)$ is less then a given value L in the interval [LAI$_{\mathrm{min}}$, LAI$_{\mathrm{max}}$].

The functions (9) and (10) are the LAI conditional distribution functions provided $p \in P_{bio}$, and validity of (6) and (7), respectively. Note that the functions (9) and (10) depend on L and neighborhoods O_A and O_r. The values

$$L_{A,bio} = \int_{LAI_{min}}^{LAI_{max}} l \, dF_{A,bio}(l) \, , \tag{11}$$

$$L_{r,A,bio} = \int_{LAI_{min}}^{LAI_{max}} l \, dF_{r,A,bio}(l) \tag{12}$$

are taken as solutions of (6) and (7), and the values

$$d_{A,bio}^2 = \int_{LAI_{min}}^{LAI_{max}} \left(L_{A,bio} - l\right)^2 dF_{A,bio}(l) \, , \tag{13}$$

$$d_{r,A,bio}^2 = \int_{LAI_{min}}^{LAI_{max}} \left(L_{r,A,bio} - l\right)^2 dF_{r,A,bio}(l) \tag{14}$$

are taken as the characteristics of the solution accuracy. If (6) and (7) have no solutions (i.e., $F=0$), we assign a default value to (13) and (14). We propose to archive (11), (12), (13), and (14) for all six biomes for diagnostic purposes.

We note some properties of the functions $F_{A,bio}$ and $F_{r,A,bio}$ which help to explain the definition of the solution (Appendix). It follows directly from definitions (9) and (10) that if the function $l(p)$ is constant, say $l(p) \equiv L^*$, when $p \in Q_A(LAI_{max}, O_A; P_{bio})$ and $p \in Q_r(LAI_{max}, O_{A,r}; P_{bio})$, then $L_{r,bio}$ and $L_{r,A,bio}$ coincide with L^*. This allows the use of three-dimensional canopy radiation models for which LAI is usually not in the model parameter list. In this case, canopy realizations can vary considerably, while LAI remains unchanged. This property shows that (11) and (12) are sensitive to LAI but not to the situations generating the value of LAI. It follows from this that if the inverse problem has a unique solution for given set of measurements, then (11) and (12) coincide with this solution. If model parameters from $Q_A(LAI_{max}, O_A; P_{bio})$ and $Q_r(LAI_{max}, O_{A,r}; P_{bio})$ can generate several values of LAI, (11) and (12) provide a weighted mean in accordance with the frequency of occurrence of a given value of LAI. The accuracy of a solution cannot be improved if no additional information is available. These properties provide convergence of the algorithm; that is, the more the measured information is available and the more accurate this information is, the more reliable and accurate the algorithm output will be.

Figures 1-4 illustrate various aspects of the function (9) and retrieval results for biome 1 (grasses and cereal crops) for 40 different neighborhoods O_A. This biome type is represented by five parameters in the algorithm [*Diner et al.*, 1998b], which include the "effective" ground reflectances $\rho_i = \rho_{q,eff}(\lambda_i)$ (section 6) in the MISR bands λ_i, $i=1, 2, 3, 4$, and LAI; that is, $p=(\rho_1, \rho_2, \rho_3, \rho_4, LAI)$. The effective ground reflection was a linear function with respect to wavelength in this example; that is, $\rho_{q,eff}(\lambda_i) = s(\lambda_1 - \lambda) + \rho_1$. The slope s, effective ground reflectance in the first MISR band ρ_1 and LAI, can vary continuously within given biome-dependent intervals $[\rho_{min}, \rho_{max}]$, $[s_{min}, s_{max}]$ and $[LAI_{min}, LAI_{max}]$. Thus the set P_{bio}, bio=1, is defined in our example as

$$P_{bio} = \big\{ (\rho, s, LAI) : \rho_{min} \leq \rho \leq \rho_{max},$$
$$s_{min} \leq s \leq s_{max}, \, LAI_{min} \leq LAI \leq LAI_{max} \big\}.$$

The function l takes the form $l(p)=LAI$ in this case. We choose 40 elements,

$$p_k=(0.025, \, 1.184 \times 10^{-4}, \, LAI_k), \, LAI_k=0.1 + (k-1) \times 0.25, \tag{15}$$

$$k=1, 2, \ldots, 40,$$

from the set P_{bio}. For each soil/LAI pattern p_k, we estimated DHR for the four MISR bands, which were taken as $\tilde{A}$ (Ω_0). The uncertainties in (5) were simulated as

$$\sigma_A^2(l) = \varepsilon^2 \, \frac{\sum_{k=1}^{4} \left[A_{\lambda_k}^{hem}(\Omega_0)\right]^2}{4} \, , \tag{16}$$

where ε is a variable in the calculations; that is, these uncertainties can be interpreted as the mean retrieved uncertainty. If the values $A_{\lambda}^{hem}(\Omega_0)$, $\lambda=\lambda_1, \lambda_2, \lambda_3, \lambda_4$, are approximately of the same order, the value of the merit function (5) using uncertainties of the individual $A_{\lambda}^{hem}(\Omega_0)$ is close to that when using (16). In the general case, the merit function using (16) describes the closeness between measured and simulated values worse than the ones using the individual uncertainties, i.e., neighborhoods O_A determined by the merit function (5) with (16) are broader than the ones accounting for individual uncertainties. One object of our study was to analyze the behavior of the parameter distribution function in situations worse than what may be realized. The parameters used in this study are as follows: the polar angle of the unit direction Ω_0 was 45^0; $\rho_{min}=0.025$, $\rho_{max}=0.070$, $s_{min}=1.184 \times 10^{-4}$, $s_{max}=1.896 \times 10^{-4}$; $LAI_{min}=0.1$; $LAI_{max}=9.85$; $f_{dir}=1$, $\varepsilon=0.20$, and $h_A=1$. The number N in (8) was 1000, which was large enough to approximate the parameter distribution functions (9) and (10) sufficiently well.

The total number, $N_A(LAI_{max}; P_{bio})$, of solutions of (6) for the 40 patterns of neighborhoods O_A are plotted in Figure 1. The neighborhoods are sorted with respect to values $l(p_k)$ where p_k is the soil/LAI pattern (15) for which O_A was simulated. Values $l(p_k)$ are shown on the horizontal axis. Figure 2 presents the numbers of different values of $l(p)$ when p ran over the set $Q_A(LAI_{max}, O_A; P_{bio})$, i.e., numbers of different values of LAI satisfying (6). Figure 3 demonstrates the functions $\Delta F_{A,bio}(L) = F_{A,bio}(L+0.25) - F_{A,bio}(L)$ for five different patterns of O_A. One can discern two types of shapes for $\Delta F_{A,bio}$. The first one localizes values of LAI sufficiently well (curves 0.1, 1, 2, and 3). They correspond to neighborhoods O_A for which $l(p) \leq 3$. The curve 5 shows that the set of p for which model results are nearly equivalent to the measurements is rather big.
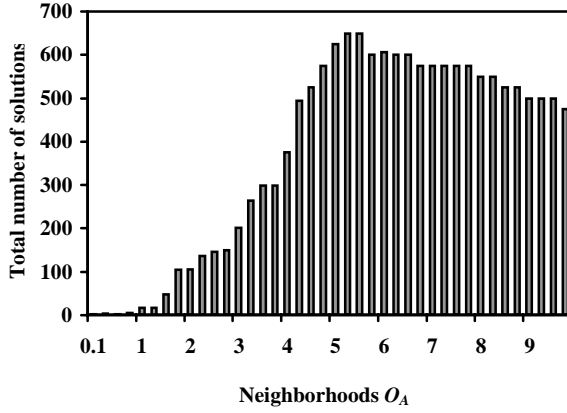
Figure. 1. Total number of solutions for 40 patterns of neighborhoods O_A. The horizontal axis shows the values $l(p_k)$, where p_k is the soil/leaf area index (LAI) pattern for which O_A was simulated.
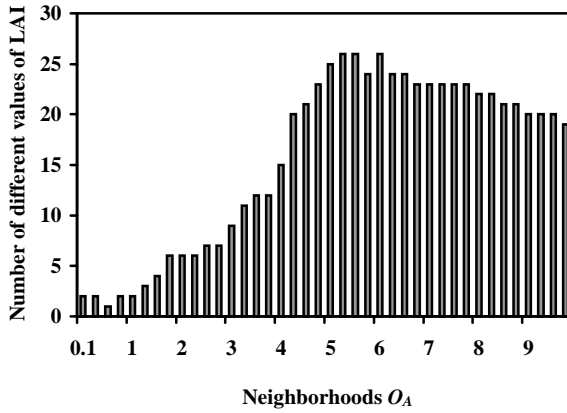
Figure 2. Number of different solutions for 40 patterns of neighborhoods O_A.
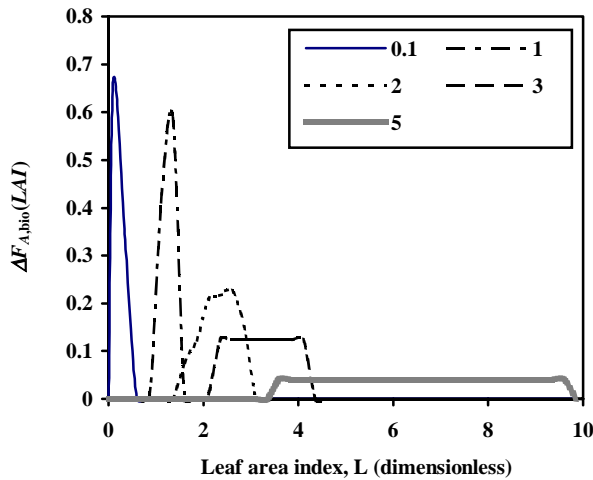
Figure 3. Localization of probable values of LAI. The function $\Delta F_{A,\mathrm{bio}}(L) = F_{A,\mathrm{bio}}(L+0.25) - F_{A,\mathrm{bio}}(L)$ shows the probability distribution of multiple acceptable solutions for five different patterns of O_A. Curve 0.1: $l(p_k)$=0.1; curve 1: $l(p_k)$=1; curve 2: $l(p_k)$=2; curve 3: $l(p_k)$=3; curve 5: $l(p_k)$=5.
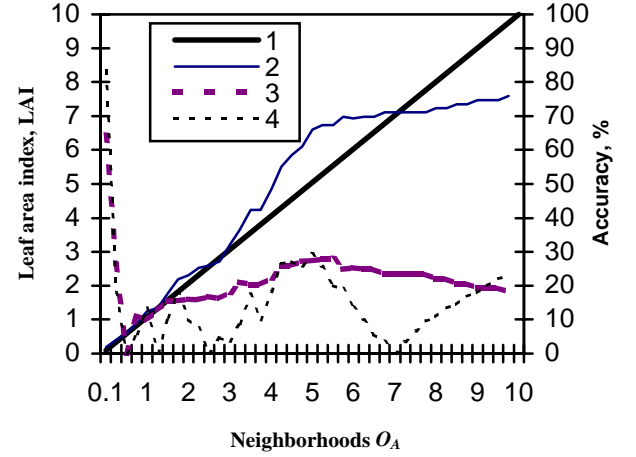
Figure 4. Comparison of the retrieved and exact solutions of the inverse problem for 40 patterns of neighborhoods O_A. Vertical axis on the left side: 1, exact solution; 2, retrieved solution. Vertical axis on the right side: 3, 100·|curve_1-curve_2|/curve_1; 4, 100·$d_{A,bio}$/curve_1.

We will quantify this situation in section 3. Figure 4 contains two plots; the first one with the vertical axis on the left side demonstrates exact (curve 1) and retrieved (curve 2) values of LAI for our patterns of O_A. The meaning of the horizontal axis is the same as in Figure 1. The second plot with the vertical axis on the right presents values $\delta_{A,\mathrm{bio}}=100\cdot d_{A,\mathrm{bio}}/L_{A,\mathrm{bio}}$ (curve 3), and $\delta_{\mathrm{LAI}}=100\cdot|\mathrm{LAI}_{\mathrm{bio}}-L_{A,\mathrm{bio}}|/\mathrm{LAI}_{\mathrm{bio}}$ (curve 4) for 40 patterns of O_A. Here $\mathrm{LAI}_{\mathrm{bio}}= l(p_k)$ is the value of leaf area index for which O_A was simulated and $L_{A,\mathrm{bio}}$ is the value obtained from (11). The value $\delta_{A,\mathrm{bio}}$ mainly varied between 11% and 28%, even in cases when the algorithm retrieves LAI accurately (compare curves 3 and 4). The range of variations in $\delta_{A,\mathrm{bio}}$, however, is comparable to the uncertainty of O_A (recall that in our example this set includes elements that differ from a given vector $\tilde{\vec{A}}^{\,\mathrm{hem}}(\Omega_0)$, on an average, by 20%). Therefore (13) can be taken as the characteristic of the inversion accuracy. However, this value is slightly sensitive to the two cases when the function (9) localizes LAI values (Figure 3, curves 0.1, 1, 2, and 3) and when such localization does not take place (curve 5). Therefore one needs an additional characteristic that distinguishes these two conditions. We must also pay attention to the case when the accuracy of the retrieved LAI exceeds the uncertainty of O_A. The neighborhood with $l(p_k)$=0.1 demonstrates such an example. In this case, N=1000 in (8) was not big enough to adequately represent the set of possible observations. There were vectors $\vec{A} \in R^4$ which are close to the simulated $\vec{A}^{\,\mathrm{hem}}(\Omega_0)$, $\vec{A} \approx \vec{A}^{\,\mathrm{hem}}(\Omega_0)$ and which were not elements of D_A.

3. Saturation Domain

Calculations presented in section 2 indicate that there may be "small" neighborhoods O_A and O_r in D_A and D_r which can be generated by a rather "wide" set of the canopy realizations. Curve 5 in Figure 3 illustrates such a condition: any p satisfy-

ing $l(p) \geq 3.5$ with equal probability can be a solution of (6). In our study, similar behavior was observed for all patterns O_A corresponding to $l(p_k) \geq 5$. The aim of this section is to quantify these situations.

Let us consider the set $S_{\text{bio}}(L^*, L)$ defined as

$$S_{\text{bio}}(L^*, L) = \left\{ p \in P_{\text{bio}} : \quad L^* \leq l(p) < L; \quad L \leq \text{LAI}_{\max} \right\}. \quad (17)$$

This set does not depend on canopy reflectances. A measured $\tilde{\vec{A}}^{\text{hem}}(\Omega_0)$ is defined to belong to the saturation domain $D_{S,A} \subseteq D_A$, and a value, $L_A^* \in [\text{LAI}_{\min}, \text{LAI}_{\max}]$, is a saturation point if

$$\left\{ p \in P_{\text{bio}} : \quad L_A^* \leq l(p) < \text{LAI}_{\max} \text{ and } \vec{A}^{\text{hem}}(\Omega_0) \in O_A \right\}$$
$$= S_{\text{bio}}(L_A^*, \text{LAI}_{\max}). \quad (18)$$

This equality shows that for given O_A, a canopy radiation model is insensitive to the canopy realizations from the set $S_{\text{bio}}(L_A^*, \text{LAI}_{\max})$. All $\tilde{\vec{A}}^{\text{hem}}(\Omega_0)$ satisfying the condition (18) constitute the saturation domain $D_{S,A}$. Figure 3 demonstrates one example of an element from the saturation domain and saturation point: the neighborhood O_A corresponding to p_{21} (see (15)) belongs to the saturation domain, and any value of LAI from 3.6 to 9.85 can be a solution with equal probability. The point $L=3.6$ is the saturation point. Similarly, a saturation domain, $D_{S,r} \subseteq D_r$ and saturation point, $L_r^* \in [\text{LAI}_{\min}, \text{LAI}_{\max}]$, for the HDRF and BRF can be introduced.

In the algorithm, the leaf area distribution function is parameterized in terms of ground cover g and mean leaf area index L of an individual tree (section 5). The ranges

$$g_{\min} \leq g \leq g_{\max}, \qquad L_{\min} \leq L \leq L_{\max}$$

of their possible variation depend on the biome type and are assumed to be known [*Knyazikhin et al.*, this issue]. Thus the function $l(p)$ has the form $l(p)=gL$, and

$$\text{LAI}_{\min} = g_{\min}L_{\min}, \qquad \text{LAI}_{\max} = g_{\max}L_{\max}. \quad (19)$$

We note that in the cases of biome 1 (grasses and cereal crops), vegetation is idealized as a horizontally homogeneous medium [*Knyazikhin et al.*, this issue]. For this biome, $g_{\min}=g_{\max}=1$. Analogous to (9) and (10), a solution distribution function for the saturation domain can be introduced as

$$\Phi(L^*, L) = \lim_{N \to \infty} \frac{N_S(L^*, L)}{N_S(L^*, \text{LAI}_{\max})},$$

where N is defined by (8) and $N_S(L^*, L)$ is the number of subsets $P_{\text{bio},k}$ containing at least one element from the set (17). Accounting for $l(p)=gL$, we get

$$\Phi(L^*, L) = \frac{\psi(L^*, L)}{\psi(L^*, \text{LAI}_{\max})}, \quad (20)$$

where the function $\psi(L^*, L)$ takes on the value 0 if $L < L^*$, and

$$\psi(L^*, L) = \int_{\substack{L^* \leq g \cdot l < L \\ L_{\min} \leq l \leq L_{\max} \\ g_{\min} \leq g \leq g_{\max}}} dH_L(l) \, dH_G(g)$$

$$= \int_{\max\left\{L_{\min}, L^*/g_{\max}\right\}}^{\min\left\{L/g_0, L_{\max}\right\}} \left[\int_{\max\left\{L^*/l, g_{\min}\right\}}^{\min\left\{L/l, g_{\max}\right\}} dH_G(g) \right] dH_L(l)$$

if $L^* \leq L < \text{LAI}_{\max}$, and

$$\psi(L^*, L) \equiv \psi(L^*, \text{LAI}_{\max})$$

$$= \int_{\max\left\{L_{\min}, L^*/g_{\max}\right\}}^{L_{\max}} \left[\int_{\max\left\{L^*/l, g_{\min}\right\}}^{g_{\max}} dH_G(g) \right] dH_L(l)$$

if $L \geq \text{LAI}_{\max}$. Note that the function (20) is expressed in the form of the Stieltjes integral, where

$$H_G(g) = \begin{cases} 0, & \text{if } g \leq g_{\min}; \\ g, & \text{if } g_{\min} < g \leq g_{\max}; \\ g_{\max}, & \text{if } g_{\max} < g. \end{cases}$$

$$H_L(l) = \begin{cases} 0, & \text{if } l \leq L_{\min}; \\ l, & \text{if } L_{\min} < l \leq L_{\max}; \\ L_{\max}, & \text{if } L_{\max} < l. \end{cases}$$

If $L_{\min} < L_{\max}$ and $g_{\min} < g_{\max}$, then the Stieltjes integral coincides with the classical integral, and $dH_L(l)=dl$, $dH_G(g)=dg$. However, if $L_{\min}=L_{\max}$ and/or $g_{\min}=g_{\max}$, the classical integral gives a value of 0, while the Stieltjes integral provides the correct value. Thus (20) specifies the distribution of LAI in the set (17) in our algorithm. Note that if LAI and model parameters are related in another manner, function (20) may take another suitable form.

If $\tilde{\vec{A}}^{\text{hem}}(\Omega_0)$ and $\tilde{\vec{r}}(\Omega_0)$ belong to the saturation domain, then L_A^* and L_r^* exist, such that

$$F_{A,\text{bio}}(L) = \Phi(L_A^*, L) \text{ and } F_{r,A,\text{bio}}(L) = \Phi(L_r^*, L)$$

for all L from $[\text{LAI}_{\min}, \text{LAI}_{\max}]$. In this case, the solutions (11) and (12) and their variance coefficients (13) and (14) can be expressed as

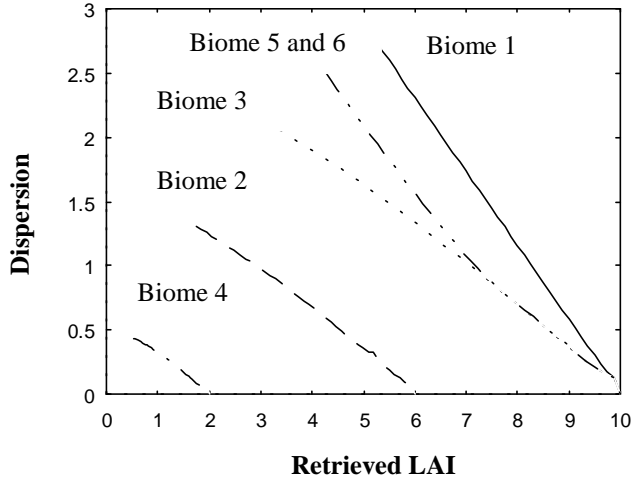$$L_{A,\text{bio}} = s_1(L_A^*), \quad d_{A,\text{bio}}^2 = s_2(L_A^*) - s_1^2(L_A^*), \quad (21)$$

$$L_{r,A,\text{bio}} = s_1(L_r^*), \quad d_{r,A,\text{bio}}^2 = s_2(L_r^*) - s_1^2(L_r^*), \quad (22)$$

where

$$s_k(L^*) = \int_{\text{LAI}_{\min}}^{\text{LAI}_{\max}} l^k \, d\Phi(L^*, l), \quad k=1,2.$$

The functions s_1 and s_2 are known and determined by canopy characteristics only and are independent of the measured

Figure 5. Saturation curves for six biomes. If the measured canopy reflectance belongs to the saturation domain, then the point (LAI, d) lies on the saturation curve. Here LAI is the retrieved value of LAI and d is its dispersion.

quantities. The set of points $[s_1(L^*), \sqrt{(s_2(L^*)-s_1^2(L^*))}]$ obtained by running L^* over $[\text{LAI}_{\min}, \text{LAI}_{\max}]$ determines a curve which is termed a saturation curve. Figure 5 demonstrates saturation curves for six biomes which correspond to canopy parameterization introduced by [*Myneni et al.*, 1997; *Knyazikhin et al.*, this issue]. These relationships allow us to formulate a necessary condition for the measured reflectances belonging to the saturation domain as follows: If $\tilde{A}^{\text{hem}}(\Omega_0) \in D_{S,A}$ and $\overline{\tilde{r}}(\Omega_0) \in D_{S,r}$ then the points $[L_{A,\text{bio}}, d_{A,\text{bio}}]$ and $[L_{r,A,\text{bio}}, d_{r,A,\text{bio}}]$ belong to saturation curves, or what amounts to the same thing, solutions of the equations $s_1(L_A)=L_{A,\text{bio}}$, $s_2(L_d)-s_1^2(L_d)=d^2_{A,bio}$ and $s_1(L_r)=L_{r,A,\text{bio}}$, $s_2(L_{r,d})-s_1^2(L_{r,d})=d^2_{r,A,bio}$ satisfy the equalities $L_A=L_d$ and $L_r=L_{r,d}$. Here the right-hand sides of these equations are evaluated during the execution of the algorithm. The left-hand sides are known functions of one variable.

This criterion takes a simple form in the case of biome 1. It follows from (20) and $g_{\min}= g_{\max}=1$ that the solution distribution function for the saturation domain in these biomes is

$$\Phi(L^*,L) = \begin{cases} 0, & \text{if } L < L^*, \\ \dfrac{L - L^*}{\text{LAI}_{\max} - L^*}, & \text{if } L^* \le L < \text{LAI}_{\max}, \\ 1, & \text{if } \text{LAI}_{\max} \le L. \end{cases}$$

Equation (21) is reduced to

$$L_{A,\text{bio}}(L_A^*) = \frac{L_A^* + \text{LAI}_{\max}}{2},$$

$$d^2_{A,\text{bio}}(L_A^*) = \frac{1}{12}\left(\text{LAI}_{\max} - L_A^*\right)^2$$

and (22) can be simplified to a similar expression, with L_A^* replaced by L_r^*. After obvious transformations, one can

express the saturation criterion for biomes 1 as follows: If $\tilde{A}^{\text{hem}}(\Omega_0) \in D_{S,A}$ and $\overline{\tilde{r}}(\Omega_0) \in D_{S,r}$, then

$$L_{A,\text{bio}} + \sqrt{3}d_{A,\text{bio}} = \text{LAI}_{\max} \quad \text{and/or}$$
$$L_{r,A,\text{bio}} + \sqrt{3}d_{r,A,\text{bio}} = \text{LAI}_{\max} \tag{23}$$

where $L_{A,\text{bio}}$, $d_{A,\text{bio}}$, $L_{r,A,\text{bio}}$, and $d_{r,A,\text{bio}}$ are evaluated from (11), (12), (13), and (14). Thus after the evaluation of LAIs and their variances, condition (23) is checked. We archive $-d_{A,\text{bio}}$ and $-d_{r,A,\text{bio}}$ if (23) is satisfied to a given accuracy. Inclusion of the minus sign means that a solution LAI was found, but the value probably belongs to the saturation domain and any value of LAI from $[2 \cdot \text{LAI}- \text{LAI}_{\max},\text{LAI}_{\max}]$ must be considered as a true solution with equal probability.

Other biome types do not allow for the formulation of the saturation criteria in a such simple form. Therefore we store saturation curves for all biomes in the look-up table. After evaluation of LAIs from (11) and (12) and their variances from (13) and (14), conditions $m(d_{A,\text{bio}},L_{A,\text{bio}})=0$ and $m(d_{r,A,\text{bio}},L_{r,A,\text{bio}})=0$ are checked. Here

$$m(d,L) = \min_{\text{LAI}_{\min} \le L^* \le \text{LAI}_{\max}}$$
$$\{[s_1(L^*) - L]^2 + [\sqrt{s_2(L^*) - s_1^2(L^*)} - d]^2\}. \tag{24}$$

We archive $-d_{A,\text{bio}}$ and $-d_{r,A,\text{bio}}$ if these relationships are fulfilled to a given accuracy.

4. Radiation Transport in a Canopy

The sets P, D_A, and D_r, which represent all possible canopy realizations and corresponding observation of canopy reflectances, are static tables in our algorithm, i.e., look-up table termed CART (canopy architecture radiative transfer) file in the MISR Algorithm Theoretical Basis Document [*Diner et al.*, 1998b]. The algorithm interacts only with elements of these sets. This provides independence from a particular canopy radiation model. A question then arises as to how the CART file has to be filled. In answering this question, we aimed (1) to minimize the size of the CART file and (2) to minimize the dependence of the CART file on a particular canopy radiation model. The aim of this section is to give a precise definition of elements of D_A and D_r.

The domain V in which a plant canopy is located is parallelepiped of dimension $X_S=Y_S=1.1$ km and biome-dependent height Z_S. The domain V can contain subdomains (or fine cells) whose size depends on the heterogeneity of the biome type. The top δV_t, bottom δV_b, and lateral δV_l surfaces of the parallelepiped form the canopy boundary, $\delta V=\delta V_t+\delta V_b+\delta V_l$. The function characterizing the radiation field is the monochromatic radiance L_λ which is a function of wavelength λ, location $r=(x,y,z)$, and direction Ω. In the absence of polarization, frequency shifting interactions, and emission processes within the canopy, the monochromatic radiance is given by the steady state radiative transfer equation,

$$\Omega \bullet \nabla L_\lambda(r,\Omega) + u_L(r)G(r,\Omega)L_\lambda(r,\Omega)$$

$$= u_L(r)\int_{4\pi}\frac{1}{\pi}\Gamma(r,\Omega'\to\Omega)L_\lambda(r,\Omega')d\Omega' + F_\lambda(r,\Omega), \quad (25)$$

where $\Omega\bullet\nabla$ is the derivative at r along the direction Ω; u_L (in m^2/m^3) is the leaf area density distribution function (leaf area per unit volume); G (dimensionless) is the mean projection of leaf normals at r on to a plane perpendicular to the direction Ω. A precise description of these variables can be found in the works of *Ross* [1981] and *Myneni* [1991]. Here we follow the formulation of [*Myneni*, 1991] for the above mentioned variables. Note that there is a term F_λ in this equation which accounts for the hot spot effect: a rather wide family of canopy radiation models are described by an equation of this form [*Knyazikhin et al.,* this issue]. The choice of F_λ depends on the model used to simulate the hot spot effect, and it is assumed to be known. We should note that F_λ may take on negative values. Thus (25) is a closed mathematical equation (not a "physical equation") and is used as the theoretical basis of an algorithm for LAI/FPAR. This type of equation also arises in reactor problems, and so we will closely follow some methods from this discipline [*Vladimirov*, 1963; *Germogenova*, 1986].

Equation (25) alone does not provide a full description of the transport process. It is necessary to specify the incident radiance at the canopy boundary δV, i.e., specification of the boundary conditions. Because the plant canopy is adjacent to the atmosphere, neighboring canopies and the soil and/or understory, all which have different reflection properties, the following boundary conditions will be used to describe the incoming radiation [*Ross et al.*, 1992]:

$$L_\lambda(r_t,\Omega) = L_{d,\lambda}^{top}(r_t,\Omega,\Omega_0) + L_{m,\lambda}^{top}(r_t)\delta(\Omega-\Omega_0), \quad (26)$$

$$r_t\in\delta V_t, \quad \Omega\bullet n_t < 0,$$

$$L_\lambda(r_l,\Omega) = \frac{1}{\pi}\int_{\Omega'\bullet n_l>0}R_{l,\lambda}(\Omega',\Omega)L_\lambda(r_l,\Omega')|\Omega'\bullet n_l|d\Omega'$$

$$+ L_{d,\lambda}^{lat}(r_l,\Omega,\Omega_0) + L_{m,\lambda}^{lat}(r_l)\delta(\Omega-\Omega_0), \quad (27)$$

$$r_l\in\delta V_l, \quad \Omega\bullet n_l < 0,$$

$$L_\lambda(r_b,\Omega) = \frac{1}{\pi}\int_{\Omega'\bullet n_b>0}R_{b,\lambda}(\Omega',\Omega)L_\lambda(r_b,\Omega')|\Omega'\bullet n_b|d\Omega', \quad (28)$$

$$r_b\in\delta V_b, \quad \Omega\bullet n_b < 0,$$

where $L_{d,\lambda}^{top}$ and $L_{m,\lambda}^{top}$ are the diffuse and monodirectional components of solar radiation incident on the top surface of the canopy boundary δV_t; Ω_0 is the direction of the monodirectional solar component; δ is the Dirac delta-function; $L_{m,\lambda}^{lat}$ is the intensity of the monodirectional solar radiation arriving at a point $r_l\in\delta V_l$ along Ω_0 without experiencing an interaction with the neighboring canopies; $L_{d,\lambda}^{lat}$ is the diffuse radiation penetrating through the lateral surface δV_l; $R_{l,\lambda}$ and $R_{b,\lambda}$ (in sr^{-1}) are the bidirectional

reflectance factors of the lateral and the bottom surfaces, respectively; and n_t, n_l, and n_b are the outward normals at points $r_t\in\delta V_t$, $r_l\in\delta V_l$, and $r_b\in\delta V_b$, respectively. A solution of the boundary value problem, expressed by (25)-(28), describes the radiation regime in a plant canopy and, as a consequence, reflectance properties of the vegetation canopy.

The hemispherical-directional reflectance factor for nonisotropic incident radiation, or HDRF, is defined as the ratio of the radiance leaving the top of the plant canopy $L_\lambda(r_t,\Omega)$, $\Omega\bullet n_t>0$ to the radiance reflected from an ideal Lambertian target into the same beam geometry and illuminated under identical atmospheric conditions [*Diner et al.*, 1998a] which can be expressed by a solution of (25)-(28) as

$$r_\lambda(\Omega,\Omega_0) = \frac{L_\lambda(r_t,\Omega)}{\frac{1}{\pi}\int_{2\pi-}L_\lambda(r_t,\Omega')|\Omega\bullet n_t|d\Omega'}, \quad \Omega\bullet n_t > 0 \ . \quad (29)$$

The bihemispherical reflectance for nonisotropic incident radiation, or BHR, is defined as ratio of the radiant exitance to the incident radiant [*Diner et al.*, 1998a]; that is,

$$A_\lambda^{hem}(\Omega_0) = \frac{\int_{2\pi+}L_\lambda(r_t,\Omega)|\Omega\bullet n_t|d\Omega}{\int_{2\pi-}L_\lambda(r_t,\Omega')|\Omega\bullet n_t|d\Omega'} \ . \quad (30)$$

The HDRF and BRF depend on the ratio f_{dir} of direct irradiance on the top of the plant canopy to the total incident irradiance. If $f_{dir}=1$, the HDRF and BHR become the bidirectional reflectance factor (BRF) and the directional hemispherical reflectance (DHR), respectively. Here $r_\lambda(\Omega,\Omega_0)$ and $A_\lambda^{hem}(\Omega_0)$ denote the HDRF and BHR ($f_{dir}\neq1$) or the BRF and DHR ($f_{dir}=1$). The MISR instrument provides this ratio, and so, it is input to the algorithm. Equations (29) and (30) depend on canopy realization $p\in P$. Evaluating (29) and (30) for all $p\in P$, one obtains the sets D_r and D_A, which contain all possible values of the HDRF and BHR.

5. Assumptions: Radiation Transfer Process

Theoretically, the sets D_A and D_r can be generated offline by solving the transport equation at four MISR spectral bands for various combination of Sun-sensor geometry and all canopy realizations from the set P. However, one can realize it only if the sets D_A and D_r can be reprocessed with minimum effort. The time required to precompute these sets is a direct function of the number of spectral channels used, combinations of Sun-sensor geometry, and elements in the set P. For example, the generation of the set D_r using this direct method takes approximately 192 computer hours of medium performance IBM RS/6000 RISC workstation [*Running et al.*, 1996]. The size of D_r containing BRFs for two spectral bands and for all six biomes is about 63 megabytes. The inclusion of more spectral bands and view directions leads to significant demands on the core memory required to execute this algorithm.

It makes this approach impractical in the case of MISR instrument. The aim of this section and section 6 is to formulate some assumptions allowing for a significant reduction in the size of D_A and D_r.

5.1. Conservativity

A radiative transfer model is defined to be conservative if the law of energy conservation holds true for any elementary volume [*Bass et al.*, 1986]. Within a conservative model, radiation absorbed, transmitted, and reflected by the canopy is always equal to radiation incident on the canopy. A rather wide family of canopy radiation models [*Kuusk*, 1985; *Marshak*, 1989; *Pinty et al.*, 1989; *Li and Strahler*, 1992; *Myneni et al.*, 1995; *Pinty and Verstraete*, 1998] which account for the hot spot are equivalent to the solution of the above boundary value problem in which the function F_λ has the following form [*Knyazikhin et al.*, this issue]:

$$F_\lambda(r,\Omega) = [\sigma(r,\Omega) - \sigma_H(r,\Omega,\Omega_0)]L_{H,\lambda}(r,\Omega).$$

Here $L_{H,\lambda}$ is the upwardly directed once-scattered radiance produced by the hot spot, and σ_H is a model-dependent total interaction cross section, introduced in canopy radiation models to account for the hot spot effect and to evaluate $L_{H,\lambda}$. The total interaction cross section σ is used to evaluate the attenuation of both direct solar radiance and multiply scattered radiance. Because F_λ can take on negative values, it has no physical meaning in terms of energy conservation. These types of canopy radiation models are mainly used to fit simulated BRFs to measured BRFs. However, the ability of a model to simulate canopy reflection is not a sufficient requisite for the solution of the inverse problem. Canopy radiation models must also satisfy the law of energy conservation and provide the correct proportions of canopy absorptance, transmittance, and reflectance. Because the retrieval algorithm is based on energy conservation, the following "minimum" requirement, which the canopy radiation models must satisfy in order to be useful for inverse problems, is formulated:

$$\int_V dr \int_{4\pi} d\Omega F_\lambda(r,\Omega) = 0 , \qquad (31)$$

for any λ. This equation does not allow a nonphysical source $F_\lambda(r,\Omega)$ to influence the canopy radiative energy balance. Currently, we use a model for σ_H proposed by *Myneni et al.* [1995]. A nonconservative canopy radiation model must be corrected, as described in section 8.

5.2. Leaf Area Index

The leaf area index LAI is defined as

$$LAI = \frac{1}{X_S Y_S} \int_V u_L(r)\, dr \ .$$

If the vegetation canopy consists of N_c individual trees, LAI can be expressed as

$$LAI = \sum_{k=1}^{N_c} g_k \frac{1}{S_k} \int_{V_k} u_L(r)\, dr = \sum_{k=1}^{N_c} g_k LAI_k \ ,$$

where S_k is the crown projection of the kth tree onto the ground; $g_k = S_k/(X_S Y_S)$ and LAI_k is the leaf area index of an individual tree. Thus LAI is $LAI = gLAI_0$, where $g = \sum_{k=1}^{N_c} g_k$ is the ground cover, and

$$LAI_0 = \frac{1}{g} \sum_{k=1}^{N_c} g_k \cdot LAI_k$$

is the mean LAI of a single tree. The spatial distribution of trees in the stand is a characteristic of the biome type and is assumed to be random. For each biome type, the leaf area density distribution function is parameterized in terms of the ground cover and mean leaf area index of an individual tree, each varying within given biome-specific intervals [g_{min}, g_{max}] and [L_{min}, L_{max}], respectively. Thus the vegetation canopy is represented as a domain V consisting of identical trees in order to numerically evaluate the transport equation.

5.3. Anisotropy of Incoming Diffuse Radiation

A model of clear-sky radiance proposed by *Pokrowski* [1929] is used to approximate the ratio between the angular distribution of incoming diffuse radiation and its flux:

$$\frac{L_{d,\lambda}^{top}(r_t,\Omega)}{\int_{2\pi-} L_{d,\lambda}^{top}(r_t,\Omega)|\mu|d\Omega} = \left[1 - \exp\left(\frac{-0.32}{|\mu|}\right)\right]\frac{1+\Omega\bullet\Omega_0}{1-\Omega\bullet\Omega_0} .$$

Here $\Omega \sim (\mu,\varphi)$ and $\mu < 0$. We assume that this ratio does not depend on wavelength. The diffuse radiation $L_{d,\lambda}^{top}$ does not depend on the top boundary space point $r_t \in \delta V_t$. This allows the parameterization of the incoming radiation field in terms of f_{dir} and the total (diffuse and direct) incident flux.

5.4. Boundary Conditions for Lateral Surface

The radiation penetrating through the lateral sides of the canopy depends on the neighboring environment. Its influence on the radiation field within the canopy is especially pronounced near the lateral canopy boundary. Therefore inaccuracies in the lateral boundary conditions may cause distortions in the simulated radiation field within the domain V. These distortions, however, decrease with distance from this boundary toward the center of the domain. The size of the "distorted area" depends on the adjoining vegetation, atmospheric conditions, and model resolution [*Kranigk*, 1996]. In particular, it has been shown that these lateral effects can be neglected when the radiation regime is analyzed in a rather extended canopy, as is the case considering the rather large MISR pixel (~1.1 km). Therefore we idealize our canopy as a horizontally infinite region. We will use a "vacuum" boundary condition for the lateral surface to numerically evaluate a solution for the case of a horizontally infinite domain,

$$L_\lambda(r_l,\Omega) = 0, \qquad r_l \in \delta V_l, \qquad \Omega \bullet n_l < 0 . \qquad (32)$$

5.5. Optical Properties of Foliage

The leaf-scattering phase function $\chi_{L,\lambda}$ is assumed to be bi-Lambertian [*Ross and Nilson*, 1968]; that is, a fraction of the energy intercepted by the foliage element is reflected or transmitted in a cosine distribution about the leaf normal,

$$\gamma_{L,\lambda}(r,\Omega_L,\Omega' \to \Omega)$$
$$= \begin{cases} \pi^{-1} r_{D,\lambda}(r) |\Omega \bullet \Omega_L|, & (\Omega \bullet \Omega_L)(\Omega' \bullet \Omega_L) < 0, \\ \pi^{-1} t_{D,\lambda}(r) |\Omega \bullet \Omega_L|, & (\Omega \bullet \Omega_L)(\Omega' \bullet \Omega_L) > 0. \end{cases}$$

Here $r_{D,\lambda}$ and $t_{D,\lambda}$ are the spectral reflectance and transmittance, respectively, of the leaf element. Figure 6 shows an example of the sensitivity of the reflection coefficient $r_{D,\lambda}$ for the 1-year shoots (*Picea abies* (L) karst) on its location in space. In spite of this spatial variation the shapes of spectral reflectance and transmittance are rather stable. For example, compared with the mean, the deviation is, on average, about 12-15%, which does not exceed the accuracy of the canopy radiation model [*Knyazikhin et al.*, 1997]. Therefore the spatial variation of foliage optical properties can be neglected. Thus the algorithm can be parameterized in terms of spectral leaf albedo, $\omega(\lambda) = r_{D,\lambda} + t_{D,\lambda}$. For each biome the mean spectral leaf albedo is stored in the CART file. The ratio $r_{D,\lambda}/\omega(\lambda)$ is also assumed to be independent of wavelength, in any given biome type. We note that the validity of the assumptions 5.3-5.5 was verified by comparing simulation results with field measurements [*Knyazikhin et al.*, 1997].

# 6. Assumptions: Ground Reflectance and Anisotropy

To parameterize the contribution of the surface underneath the canopy (soil or/and understory) to the canopy radiation regime, an effective ground reflectance is introduced, namely,

$$\rho_{q,\text{eff}}(r_b,\lambda) = \frac{\int\limits_{2\pi-}\int\limits_{2\pi+} R_{b,\lambda}(\Omega',\Omega) |\mu\mu'| L_\lambda(r_b,\Omega') d\Omega d\Omega'}{\pi \int\limits_{2\pi-} q(\Omega') |\mu'| L_\lambda(r_b,\Omega') d\Omega'} .$$

Here L_λ is the solution of the boundary value problem for the transport equation; $r_b \in \delta V_b$ and $\Omega \bullet n_b < 0$. The function q is a configurable function used to better account for features of biomes [*Knyazikhin et al.*, this issue], and it satisfies the following condition:

$$\int\limits_{2\pi^-} q(\Omega') d\Omega' = 1 .$$

The effective ground reflectance depends on the canopy structure and the incident radiation field. It follows from the definition that the variation of $\rho_{q,\text{eff}}$ satisfies the following inequality:
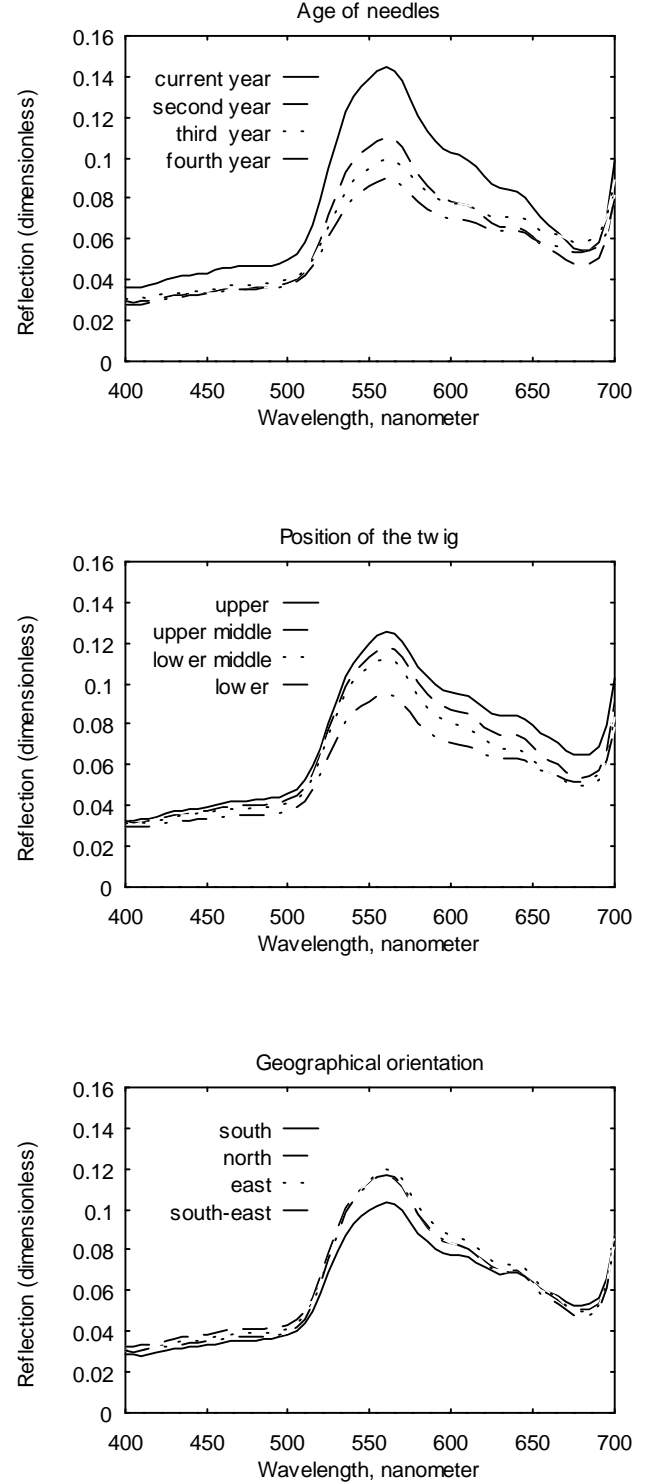
Figure 6. Spectral reflectance of 1-year-old spruce shoots. Three characteristics of the 1-year shoots were chosen to examine the spatial variations of foliage spectral properties, age of needles on the 1-year shoot; position within the tree crown (top, two middle, and bottom) and geographical orientation with respect to the tree stem (south, north, east and west).

$$\min_{\Omega'\in 2\pi-} \frac{\int\limits_{2\pi+} R_{b,\lambda}(\Omega',\Omega)|\mu|d\Omega}{\pi q(\Omega')} \le \rho_{q,\text{eff}}(r_b,\lambda)$$

$$\le \max_{\Omega'\in 2\pi-} \frac{\int\limits_{2\pi+} R_{b,\lambda}(\Omega',\Omega)|\mu|d\Omega}{\pi q(\Omega')} \; ;$$

that is, the range of variation depends on the integrated bidirectional reflectance factor of the ground surface only. For each biome type, the bidirectional reflectance factor of the ground surface $R_{b,\lambda}$ and the effective ground reflectance are assumed to be horizontally homogeneous; that is, they do not depend on the spatial point r_b. Effective ground reflectances at the MISR spectral bands are elements of the canopy realization $p \in P$. Various patterns of the spectral ground reflectance evaluated from the soil reflectance model of *Jacquemoud et al.* [1992] are included in the present version of the CART file.

To account for the anisotropy of the ground surface, we introduce an effective ground anisotropy S_q,

$$S_q(r_b,\Omega) = \frac{1}{\rho_{q,\text{eff}}(\lambda)} \frac{\int\limits_{2\pi-} R_{b,\lambda}(\Omega',\Omega)|\mu'|L_\lambda(r_b,\Omega')d\Omega'}{\pi \int\limits_{2\pi-} q(\Omega')|\mu'|L_\lambda(r_b,\Omega')d\Omega'} \; , \quad (33)$$

$$r_b \in \delta V_b, \qquad \Omega \bullet n_b < 0.$$

The effective ground anisotropy S_q depends on the canopy structure as well as the incoming radiation field. We note the following property:

$$\int\limits_{2\pi+} S_q(r_b,\Omega)|\mu|d\Omega = 1 \; ; \quad (34)$$

that is, the integral (34) depends neither on spatial nor on spectral variables. For each biome type, the effective ground anisotropy is assumed to be wavelength independent. A detailed specification of this variable is presented by *Knyazikhin et al.* [this issue]. The ground anisotropy is used to precompute some solutions of the transport equation and thus is not stored in the CART file.

7. Basic Algorithm Equations

Under the assumptions listed above, the solution of the boundary value problem for the transport equation can be expressed as [*Knyazikhin et al.*, this issue]

$$L_\lambda(r,\Omega)$$

$$\approx L_{bs,\lambda}(r,\Omega) + \frac{\rho_{q,\text{eff}}(\lambda)}{1-\rho_{q,\text{eff}}(\lambda)r_{q,\lambda}} T^q_{bs,\lambda}(\Omega_0)L_{q,\lambda}(r,\Omega) . \; (35)$$

Here $L_{bs,\lambda}$ is the solution of the "black-soil problem" which satisfies (25) with the boundary conditions expressed by (26), (32), and

$$L_{bs,\lambda}(r_b,\Omega) = 0, \qquad r_b \in \delta V_b, \qquad \Omega \bullet n_b < 0 \; .$$

The function $L_{q,\lambda}$ satisfies (25) with $F_\lambda = 0$, and the boundary conditions (32) and

$$L_{q,\lambda}(r_t,\Omega) = 0, \qquad r_t \in \delta V_t, \qquad \Omega \bullet n_t < 0 \; ,$$

$$L_{q,\lambda}(r_b,\Omega) = S_q(r_b,\Omega), \qquad r_b \in \delta V_b, \qquad \Omega \bullet n_b < 0 \; .$$

It describes the radiation regime in the plant canopy generated by an anisotropic, heterogeneous source S_q defined by (33) located at the bottom of the canopy. We term the problem of finding $L_{q,\lambda}$ the "S problem." Further,

$$T^q_{bs,\lambda}(\Omega_0) = \left\langle \int\limits_{2\pi-} q(\Omega')L_{bs,\lambda}(r_b,\Omega')|\mu'|d\Omega' \right\rangle ;$$

$$r_{q,\lambda}(r_b) = \left\langle \int\limits_{2\pi-} q(\Omega')L_{q,\lambda}(r_b,\Omega')|\mu'|d\Omega' \right\rangle ;$$

where the angle brackets denote the mean over the ground surface. Note that we can replace the approximate equality in (35) by an exact equality if a one-dimensional canopy radiation model is used to evaluate the radiative regime in plant canopy. It follows from (35), (29), and (30) that the BHR, $A^{hem}_\lambda(\Omega_0)$, the HDRF, r_λ, and the fraction of radiation absorbed by the vegetation $\mathbf{a}^{hem}_\lambda$ at wavelength λ can be expressed as

$$A^{hem}_\lambda(\Omega_0) \approx \mathbf{r}^{hem}_{bs,\lambda}(\Omega_0) + \mathbf{t}_{q,\lambda} \frac{\rho_{q,\text{eff}}(\lambda)}{1-\rho_{q,\text{eff}}(\lambda)r_{q,\lambda}} \mathbf{t}^{hem,q}_{bs,\lambda}(\Omega_0) \; ,$$

$$(36)$$

$$r_\lambda(\Omega,\Omega_0) \approx$$

$$r_{bs,\lambda}(\Omega,\Omega_0) + \pi\tau_{q,\lambda}(\Omega)\frac{\rho_{q,\text{eff}}(\lambda)}{1-\rho_{q,\text{eff}}(\lambda)r_{q,\lambda}} \mathbf{t}^{hem,q}_{bs,\lambda}(\Omega_0),$$

$$(37)$$

$$\mathbf{a}^{hem}_\lambda(\Omega_0) \approx \mathbf{a}^{hem}_{bs,\lambda}(\Omega_0) + \mathbf{a}_{q,\lambda}\frac{\rho_{q,\text{eff}}(\lambda)}{1-\rho_{q,\text{eff}}(\lambda)\cdot r_{q,\lambda}} \mathbf{t}^{hem,q}_{bs,\lambda}(\Omega_0) \; ,$$

$$(38)$$

where $\mathbf{r}^{hem}_{bs,\lambda}$, $r_{bs,\lambda}$, and $\mathbf{a}^{hem}_{bs,\lambda}$ are the BHR, HDRF, and the fraction of radiation absorbed by the vegetation, respectively, when the effective ground reflectance is zero. Here

$$\mathbf{t}^{hem,q}_{bs,\lambda}(\Omega_0) = \frac{T^q_{bs,\lambda}(\Omega_0)}{\int\limits_{2\pi-} |\mu'|L_\lambda(r_t,\Omega')d\Omega'}$$

is the weighted canopy transmittance,

$$\mathbf{t}_{q,\lambda} = \int\limits_{2\pi+} |\mu'|L_{q,\lambda}(r_t,\Omega')d\Omega'$$

is the transmittance resulting from the anisotropic source S_q located underneath the canopy,

$$\tau_{q,\lambda}(\Omega) = L_{q,\lambda}(r_{\rm t},\Omega)$$

is the radiance generated by S_q which leaves the plant canopy at the top, and $\mathbf{a}_{q,\lambda}$ is the fraction of radiation generated by S_q and absorbed by the vegetation. The radiation reflected, transmitted, and absorbed by the vegetation must be related via the law of energy conservation:

$$\mathbf{r}_{{\rm bs},\lambda}^{\rm hem} + k_{q,\lambda}(\Omega_0)\mathbf{t}_{{\rm bs},\lambda}^{{\rm hem},q} + \mathbf{a}_{{\rm bs},\lambda}^{\rm hem} = 1, \; k_{q,\lambda}(\Omega_0) = \frac{\mathbf{t}_{{\rm bs},\lambda}^{{\rm hem},q\equiv1}(\Omega_0)}{\mathbf{t}_{{\rm bs},\lambda}^{{\rm hem},q}(\Omega_0)},$$

(39)

$$\mathbf{r}_{q,\lambda} + \mathbf{t}_{q,\lambda} + \mathbf{a}_{q,\lambda} = 1 \; . \qquad (40)$$

Note that all variables in (36) and (37) are mean values averaged over the top surface of the canopy.

It follows from (36) that

$$A_\lambda^{\rm hem}(\Omega_0) - \mathbf{r}_{{\rm bs},\lambda}^{\rm hem}(\Omega_0) \approx \mathbf{t}_{q,\lambda}\frac{\rho_{q,{\rm eff}}(\lambda)}{1-\rho_{q,{\rm eff}}(\lambda)\mathbf{r}_{q,\lambda}}\mathbf{t}_{{\rm bs},\lambda}^{{\rm hem},q}(\Omega_0) \; .$$

(41)

This equation shows that the contribution of the canopy ground surface to the canopy-leaving radiance is proportional to the square of the canopy transmittance, and the factor of proportionality depends on the effective ground reflectance. If the right side is sufficiently small, we can neglect this contribution.

We have expressed the solution of the transport problem in terms of the effective ground reflectance, and solutions of the "black-soil problem" and the "S problem." The solution of the "black-soil problem" depends on Sun-view geometry, canopy architecture, and spectral properties of the leaves. The "S problem" depends on the spectral properties of the leaves and canopy structure only! These properties allow a significant reduction in the size of the CART file because there is no need to store the dependence of the exiting radiation on ground reflection properties. Elements of D_r and D_A can be composed from precomputed solutions of the "black-soil problem" and "S problem" and precomputed values of the effective ground reflectance.

8. Conservativity As a Tool to Constrain Retrieval

In spite of the diversity of canopy reflectance models, their direct use in an inversion algorithm is ineffective. In the case of forests, for example, the interaction of photons with the rough and rather thin surface of tree crowns and with the ground in between the crowns are the most important factors causing the observed variation in the directional reflectance distribution. These phenomena are rarely captured by many canopy reflectance models. As a result, these models are only slightly sensitive to the within-canopy radiation regime. This assertion is based on the fact that a rather wide family of canopy radiation models are solutions to (25), including model-dependent nonphysical internal source F_λ [*Knyazikhin*

et al., this issue]. Within such a model the radiation absorbed, transmitted, and reflected by the canopy is not equal to the radiation incident on the canopy. The function F_λ is chosen such that the model simulates the reflected radiance correctly; that is, these models account for photon interactions within a rather small domain of the vegetation canopy. On the other hand, it is the within-canopy radiation regime that is sensitive to the canopy structure and therefore to LAI. The within-canopy radiation regime also determines the amount of solar energy absorbed by the vegetation. Ignoring this phenomenology in canopy radiation models leads to a large number of nonphysical solutions when one inverts a canopy reflectance model. It may even be that that the saturation domain coincides with D_r and D_A. Therefore (36) and (37) must be transformed before they can be used in a retrieval algorithm.

Let us introduce the required weights

$$w_{{\rm bs},\lambda}(\Omega,\Omega_0) = \frac{r_{{\rm bs},\lambda}(\Omega,\Omega_0)}{\pi\mathbf{r}_{{\rm bs},\lambda}^{\rm hem}(\Omega_0)}, \quad \int_{2\pi^+}w_{{\rm bs},\lambda}(\Omega,\Omega_0)|\mu|\,d\Omega = 1 \; ,$$

(42)

$$w_\lambda^q(\Omega) = \frac{\tau_\lambda^q(\Omega)}{\mathbf{t}_{q,\lambda}}, \quad \int_{2\pi^+}w_\lambda^q(\Omega)|\mu|\,d\Omega = 1 \; . \qquad (43)$$

$$\Omega\bullet{\rm n}_{\rm t} < 0 \; .$$

With this notation, (37) can be rewritten as

$$r_\lambda(\Omega,\Omega_0) \approx \pi w_{{\rm bs},\lambda}\mathbf{r}_{{\rm bs},\lambda}^{\rm hem}(\Omega_0)$$

$$+ \pi w_\lambda^q\mathbf{t}_{q,\lambda}\frac{\rho_{q,{\rm eff}}(\lambda)}{1-\rho_{q,{\rm eff}}(\lambda)\mathbf{r}_{q,\lambda}}\mathbf{t}_{{\rm bs},\lambda}^{{\rm hem},q}(\Omega_0) \qquad (44)$$

and from (39) and (40) the canopy reflectances $\mathbf{r}^{\rm hem}{}_{{\rm bs},\lambda}$ and $\mathbf{r}_{q,\lambda}$ can be written as

$$\mathbf{r}_{{\rm bs},\lambda}^{\rm hem} = 1 - \mathbf{t}_{{\rm bs},\lambda}^{{\rm hem},q\equiv1} - \mathbf{a}_{{\rm bs},\lambda}^{\rm hem} \; , \qquad (45)$$

$$\mathbf{r}_{q,\lambda} = 1 - \mathbf{t}_{q,\lambda} - \mathbf{a}_{q,\lambda} \; . \qquad (46)$$

Thus (44) is sensitive both to factors determining the directional reflectance distribution of plant canopies (the weight $w_{{\rm bs},\lambda}$) and to the within-canopy radiation regime ($\mathbf{t}_{{\rm bs},\lambda}^{{\rm hem},q\equiv1}, \mathbf{a}_{{\rm bs},\lambda}^{\rm hem}, \mathbf{t}_{q,\lambda}, \mathbf{a}_{q,\lambda}$). Equations (44)-(46) also allow the formulation of a test for the "eligibility" of a canopy radiation model to generate the CART. First the weight $w_{{\rm bs},\lambda}$ is evaluated as a function of Sun-view geometry, wavelength, and LAI by using a field-tested canopy reflectance model. Then, with the same model, $\mathbf{r}^{\rm hem}{}_{{\rm bs},\lambda}$ and $\mathbf{r}_{q,\lambda}$ are evaluated from (45) and (46) and inserted into (42). A canopy radiation model is "eligible" to generate the CART file if (42) is satisfied to within a given accuracy for any Sun-view combination, wavelength, and LAI. The requirement (31) is necessary to satisfy this test. However, it is not a sufficient condition to provide the correct proportion among canopy absorptance, transmittance, and reflectance.

We do not know of a canopy reflectance model which can pass the above test. It is because there is no published model thus far which satisfies the energy conservation law. Although a conservative transport equation for a vegetation canopy has not yet been formulated, one can derive some properties of the solutions of this equation [*Knyazikhin et al.*, this issue]. The following properties of the canopy spectral absorptance and transmittance [*Knyazikhin et al.*, this issue] are used to correct existing canopy radiation models: Let $\mathbf{a}(\lambda)$ and $\mathbf{t}(\lambda)$ be the fraction of radiation absorbed and transmitted by the vegetation at wavelength λ for either the "black-soil problem" or the "S problem." The following relationships are valid in both cases:

$$\mathbf{a}(\lambda) = \frac{1 - \gamma_0(\lambda_0)}{1 - \gamma_0(\lambda)} \frac{1 - \omega(\lambda)}{1 - \omega(\lambda_0)} \mathbf{a}(\lambda_0), \qquad (47)$$

$$\mathbf{t}\left(\lambda, \frac{r_D(\lambda)}{\omega(\lambda)}\right) = \frac{1 - \gamma_0(\lambda_0)}{1 - \gamma_0(\lambda)} \mathbf{t}\left(\lambda_0, \frac{r_D(\lambda_0)}{\omega(\lambda_0)}\right), \qquad (48)$$

where $\gamma_0(\lambda) = \omega(\lambda)[1 - \exp(-K)]$ is the unique positive eigenvalue of the transport equation, r_D is the spectral leaf reflectance, and ω is the leaf albedo [*Knyazikhin et al.*, this issue]. Note that in the case of the "black-soil problem" these relationships are valid for the radiation regime, which is the sum of the radiation fields generated by the direct and diffuse components of incident solar radiation. The coefficient K may depend on canopy structure (i.e., biome type, ground cover, etc.) and Sun position but not on wavelength or soil type. Its specification depends on the parameter type (absorptance or transmittance) and the type of transport problem ("black-soil" or "S problem"). This coefficient, however, does not depend on the type of the transport problem and Sun position when it refers to canopy absorptance. In the case of canopy transmittance it depends on the ratio r_D/ω, which is assumed to be wavelength independent (section 5.5). Thus given $\mathbf{a}$ and $\mathbf{t}$ at wavelength λ_0, we can evaluate these variables at any other wavelength λ. These properties can be used to specify correct values of canopy absorptance and transmittance. We introduce the coefficients $\mathbf{pt}_{bs}$, $\mathbf{pt}_q$, and $\mathbf{pa}$ which are equal to $[1 - \exp(-K)]$, with the appropriate coefficient K for the transmittances of the "black-soil problem," the "S problem," and the canopy absorptance, respectively. Note that the eigenvalue γ_0 depends on values of spectral leaf albedo, which in turn depends on wavelength. It allows us to parameterize the canopy absorptance and transmittance in terms of canopy structure, Sun position, and leaf albedo.

The coefficient $\mathbf{pa}$, for LAI equal to lai, is the value of x which minimizes the expression

$$\xi_{\mathbf{a}}(x, lai, \omega^*) = \int_0^1 \left[\frac{(1 - \omega^* x)(1 - \omega)}{(1 - \omega x)(1 - \omega^*)} \mathbf{a}(lai, \omega^*) - \mathbf{a}(lai, \omega) \right]^2 d\omega. \qquad (49)$$

Here $\mathbf{a}$ is the canopy absorptance which is a function of leaf albedo ω and leaf area index lai and is evaluated by solving

the transport equation. Value ω^* is a reference leaf albedo which is specified below. Note that LAI is parameterized in terms of ground cover and mean leaf area index of an individual tree; that is, $lai = gL$. Therefore we distinguish between equal values of LAI corresponding to different values of g and L in the algorithm.

In a similar fashion the coefficient $\mathbf{pt}_{bs}$ or $\mathbf{pt}_q$ is the value of x which minimizes the expression

$$\xi_{\mathbf{t},\chi}(x, lai, \omega^*) = \int_0^1 \left[\frac{1 - \omega^* x}{1 - \omega x} \mathbf{t}_\chi(lai, \omega^*) - \mathbf{t}_\chi(lai, \omega) \right]^2 d\omega$$

$$+ \int_0^1 \left[1 - \frac{1 - \omega^* x}{1 - \omega x} \mathbf{t}_\chi(lai, \omega^*) \right.$$

$$\left. - \frac{1 - \omega^* \mathbf{pa}(lai)}{1 - \omega \, \mathbf{pa}(lai)} \frac{1 - \omega^*}{1 - \omega} \mathbf{a}(lai, \omega^*) \right]^2 d\omega. \qquad (50)$$

Here $\mathbf{t}_\chi$ is the canopy transmittance for the "black-soil problem" or the "S problem," which is a function of leaf albedo ω and leaf area index lai, and is evaluated by solving the transport equation. The values $\mathbf{pt}_{bs}$ and $\mathbf{pt}_q$ for which $\xi_{\mathbf{t},bs}$ and $\xi_{\mathbf{t},q}$ attain their minimum provide the best agreement to (48) and to the energy conservation laws (45) and (46).

As a reference leaf albedo, we take such ω^* which minimizes the expression

$$\xi(\omega^*) = \int_{LAI_{min}}^{LAI_{max}} \xi_{\mathbf{a}}(\mathbf{pa}(lai), lai, \omega^*) \, d\,lai$$

$$+ \int_{LAI_{min}}^{LAI_{max}} \xi_{\mathbf{t},bs}(\mathbf{pt}_{bs}(lai), lai, \omega^*) \, d\,lai$$

$$+ \int_{LAI_{min}}^{LAI_{max}} \xi_{\mathbf{t},q}(\mathbf{pt}_q(lai), lai, \omega^*) \, d\,lai, \qquad (51)$$

where LAI_{min} and LAI_{max} are defined by (19). From our studies, optimum values of the reference leaf albedo for our canopy radiation model are 0.1, 0.26 and 0.34. A canopy radiation model is recognized as "eligible" if $\xi(\omega^*)$ defined by (51) is less then 0.001 (we achieved this value by using our model). Note that there is no conflict with the energy conservation law in the case of the "S problem." We also note that problems (49)-(51) have to be classified as ill-posed problems, and so a special technique, for example, *Tikhonov and Arsenin* [1986], is needed to resolve them.

It follows from (36) and (44) that the HDRF can be represented as

$$r_\lambda(\Omega, \Omega_0) \approx \pi w_{bs,\lambda} \mathbf{r}_{bs,\lambda}^{hem}(\Omega_0) + \pi w_\lambda^q [\tilde{A}_\lambda^{hem}(\Omega_0) - \mathbf{r}_{bs,\lambda}^{hem}(\Omega_0)]. \qquad (52)$$

We use (36) and (52) with $f_{dir} = 1$ to build the functions (9) and (10).

Thus the BHR described by (36) and the HDRF described by (52) can be expressed in terms of optical properties of a leaf and the energy conservation law, as well as in terms of solutions of the "black-soil problem" and the "S problem" at a reference leaf albedo value of ω^*. This facilitates comparison of spectral values of the BHR or HDRF with spectral properties of individual leaves, which is a rather stable characteristic of a green leaf. It also can be interpreted as "inclusion of additional information" into the algorithm, thus allowing a significant reduction in the number of retrieved solutions.

9. Description of FPAR Retrieval

It follows from (38) and (41) that the fractional amount of incident photosynthetically active radiation (PAR) absorbed by the vegetation canopy (FPAR) can be evaluated as

$$\mathrm{FPAR}(\mathrm{bio}, p, \Omega_0) = \frac{Q_{\mathrm{bs}}(\mathrm{bio}, p, \Omega_0) + Q^q(\mathrm{bio}, p, \Omega_0)}{E(\Omega_0)} \ , \quad (53)$$

where

$$Q_{\mathrm{bs}}(\mathrm{bio}, p, \Omega_0) = \int\limits_{400\mathrm{nm}}^{700\mathrm{nm}} \mathbf{a}_{\mathrm{bs},\lambda}^{\mathrm{hem}}(\Omega_0) E_{0,\lambda} e_\lambda^{\mathrm{hem}}(\Omega_0)\, d\lambda \ , \quad (54)$$

$$
\begin{aligned}
& Q^q(\mathrm{bio}, p, \Omega_0) \\
&= \int\limits_{400\mathrm{nm}}^{700\mathrm{nm}} \mathbf{a}_{q,\lambda}(\Omega_0) \frac{\rho_{q,\mathrm{eff}}(\lambda)}{1 - \rho_{q,\mathrm{eff}}(\lambda)\mathbf{r}_{q,\lambda}} \mathbf{t}_{\mathrm{bs},\lambda}^{\mathrm{hem},q} E_{0,\lambda} e_\lambda^{\mathrm{hem}}(\Omega_0)\, d\lambda \\
&= \int\limits_{400\mathrm{nm}}^{700\mathrm{nm}} \frac{\mathbf{a}_{q,\lambda}(\Omega_0)}{\mathbf{t}_{q,\lambda}(\Omega_0)} \Big[\tilde{A}_\lambda^{\mathrm{hem}}(\Omega_0) - \mathbf{r}_{bs,\lambda}^{\mathrm{hem}}(\Omega_0)\Big] E_{0,\lambda} e_\lambda^{\mathrm{hem}}(\Omega_0)\, d\lambda,
\end{aligned}
$$
$$\quad (55)$$

$$E(\Omega_0) = \int\limits_{400}^{700} E_{0,\lambda} e_\lambda^{\mathrm{hem}}(\Omega_0)\, d\lambda \ . \quad (56)$$

The Q_{bs} term describes the absorption within the canopy for the case of a black ground, and Q^q describes additional absorption within the canopy due to the interaction between the ground (soil or/and understory) and the canopy. Here $p \in P_{\mathrm{bio}}$; $E_{0,\lambda}$ is the solar irradiance spectrum known for all wavelengths; e_λ^{hem} is the normalized incident irradiance, defined as the ratio of the radiant energy incident on the surface to $E_{0,\lambda}$ [*Diner et al.*, 1998a]. The normalized incident irradiance and the BHR are provided by the MISR instrument at three spectral bands within the PAR region. We assume a piecewise linear variation in these variables over regions [446nm, 558 nm], [558 nm, 672 nm], and constant over regions [400 nm, 446 nm], [672 nm, 700 nm], i.e., letting C_λ represent either e_λ^{hem} or $\tilde{A}_\lambda^{\mathrm{nem}}$:

$$C_\lambda = \begin{cases} C_1, & \text{if } 400 \leq \lambda < \lambda_1, \\ C_1 + (\lambda - \lambda_1)(C_2 - C_1)/(\lambda_2 - \lambda_1), & \text{if } \lambda_1 \leq \lambda < \lambda_2, \\ C_2 + (\lambda - \lambda_2)(C_3 - C_2)/(\lambda_3 - \lambda_2), & \text{if } \lambda_2 \leq \lambda < \lambda_3, \\ C_3, & \text{if } \lambda_3 \leq \lambda \leq 700, \end{cases}$$
$$\quad (57)$$

where the subscripts 1, 2, and 3 denote the blue, green, and red bands, respectively. Substituting (57) into (54), (55), and (56) as well as accounting for (47), one can express $E(\Omega_0)$, Q_{bs}, and Q^q as a linear combination of e_λ^{hem} and $\tilde{A}_\lambda^{\mathrm{nem}} e_\lambda^{\mathrm{hem}}$, $\lambda = \lambda_1, \lambda_2, \lambda_3$. Coefficients of the linear combinations are precomputed and stored in the CART file. A detailed description of a final expression for (53) is presented by *Diner et al.* [1998a]. Note that the dependence of FPAR on ground reflection properties is included in $\tilde{a}_\lambda^{\mathrm{nem}}$, which is provided by the MISR instrument; that is, expression (53) is a function of biome type, ground cover g, mean leaf area index of an individual plant L, and $\tilde{a}_\lambda^{\mathrm{nem}}$. The mean over those values of g and L, which passed the first test (6), is taken as the estimate of FPAR; that is,

$$\mathrm{FPAR}_{A,\mathrm{bio}} = \frac{1}{N_{g,L}} \sum_{k=1}^{N_{g,L}} \mathrm{FPAR}(\mathrm{bio}, g_k, L_k) \ ,$$

where $N_{g,L}$ is the number of g and L values, which satisfy (6). When (6) has no solution (i.e., $F_{A,\mathrm{bio}}=0$), the algorithm defaults to a NDVI-FPAR regression analysis to obtain an estimate of FPAR [*Myneni et al*, 1997].

10. Flow of MISR LAI/FPAR Algorithm

The LAI retrieval algorithm first determines if the 1.1 km subregion has a meaningful amount of vegetation by calculating the normalized difference vegetation index (NDVI) using the previously retrieved DHRs in the red and near-IR bands. If the NDVI is less or equal to a threshold value, the subregion is classified as barren, and no additional processing is performed for LAI. Otherwise, for each biome-specific canopy realization $p_{mk}=(\rho_{m,1}, \rho_{m,2}, \rho_{m,3}, \rho_{m,4}, \mathrm{LAI}_k)$, condition (6) is checked. Here $\rho_{m,i}$, $m=1, 2, \ldots, N_\rho$, are patterns of the effective ground reflectances in the MISR bands λ_i, $i=1, 2, 3, 4$ (section 6). The value of LAI tested is given by

$$\mathrm{LAI}_k = \left[L_{\min} + (l-1)\frac{L_{\max} - L_{\min}}{N_L - 1} \right]$$
$$\times \left[g_{\min} + (j-1)\frac{g_{\max} - g_{\min}}{N_g - 1} \right],$$

$$l = 1, \cdots, N_L, \ j = 1, \cdots, N_g \ ,$$

where the LAI index $k=(j-1)N_L+l$, and $L_{\min}$, $L_{\max}$, $g_{\min}$, $g_{\max}$ are defined in section 5.2. The biome-dependent parameters $\rho_{m,i}$, $L_{\min}$, $L_{\max}$, $g_{\min}$, $g_{\max}$, N_ρ, N_L, and N_g are found in the CART file. The number N in (8), which determines the accuracy of

the approximation of $F_{A,\text{bio}}$, and $F_{r,A,\text{bio}}$, is $N_\rho N_L N_g$. Let L_k, $k=1$, $2, \ldots, N_{\text{LAI}}$ be the set of different values of LAI_k. For each biome type we now compute a histogram $N_1(L_k)$ as the count of how many times the value L_k passed the condition (6). The total number of valid solutions after completion of this test is

$$N_{\text{sol},1} = \sum_{k=1}^{N_{\text{LAI}}} N_1(L_k) \, .$$

For those biomes in which $N_{\text{sol},1}>0$, we now compute mean LAI (11) and a measure of the spread in LAI (13) values for each biome from

$$L_{A,\text{bio}} = \frac{\displaystyle\sum_{k=1}^{N_{\text{LAI}}} N_1(L_k) L_k}{N_{\text{sol},1}} \, ,$$

$$d_{A,\text{bio}}^2 = \frac{\displaystyle\sum_{k=1}^{N_{\text{LAI}}} N_1(L_k)(L_k - L_{A,\text{bio}})^2}{N_{\text{sol},1}} \, .$$

After evaluation of these variables, conditions $m(d_{A,\text{bio}}, L_{A,\text{bio}})=0$ is checked. The value of $d_{A,\text{bio}}$ is replaced by $-d_{A,\text{bio}}$ if this condition is fulfilled to the given accuracy ε_d, which is stored in the CART file. Here the biome-dependent function $m(d,L)$ is defined by (24) and is found in the CART file. The parameters $N_{\text{sol},1}$, $L_{A,\text{bio}}$, and $d_{A,\text{bio}}$ are archived for each biome type. Only those p_{mk} which pass condition (6) are subject to the second step, which is the test of condition (7). This comparison test is performed in a similar manner.

Equations (36) and (52) are used to evaluate the BHR and HDRF for given p_{mk}. The biome-dependent coefficients $w_{\text{bs},\lambda}$ and w^q_λ defined by (42) and (43), respectively, are elements of the CART file. The canopy reflectances $\mathbf{r}^{\text{hem}}_{\text{bs},\lambda}$ and $\mathbf{r}_{q,\lambda}$ are evaluated from (45) and (46). The variables $\mathbf{t}^{\text{hem},q\equiv1}_{\text{bs},\lambda}$, $\mathbf{a}^{\text{hem}}_{\text{bs},\lambda}$, $\mathbf{t}_{q,\lambda}$, and $\mathbf{a}_{q,\lambda}$ depend on the spectral leaf albedo and can be expressed as (section 8, (47) and (48))

$$\mathbf{t}^{\text{hem},q\equiv1}_{\text{bs},\lambda} = f_{\text{dir},\lambda}(\Omega_0) \frac{1 - \omega^* \mathbf{pt}_{\text{bs,dir}}}{1 - \omega(\lambda)\mathbf{pt}_{\text{bs,dir}}} \mathbf{t}^{\text{hem}}_{\text{bs,dir}}(\omega^*)$$
$$+ \left[1 - f_{\text{dir},\lambda}(\Omega_0)\right] \frac{1 - \omega^* \mathbf{pt}_{\text{bs,dif}}}{1 - \omega(\lambda)\mathbf{pt}_{\text{bs,dif}}} \mathbf{t}^{\text{hem}}_{\text{bs,dif}}(\omega^*) \, ,$$

$$\mathbf{t}_{q,\lambda} = \frac{1 - \omega^* \mathbf{pt}_q}{1 - \omega(\lambda)\mathbf{pt}_q} \mathbf{t}^q(\omega^*) \, ,$$

$$\mathbf{a}^{\text{hem}}_{\text{bs},\lambda} = \frac{1 - \omega^* \mathbf{pa}}{1 - \omega(\lambda)\mathbf{pa}} \frac{1 - \omega(\lambda)}{1 - \omega^*}$$
$$\times \left\{ f_{\text{dir},\lambda}(\Omega_0) \mathbf{a}^{\text{hem}}_{\text{bs,dir}}(\omega^*) + \left[1 - f_{\text{dir},\lambda}(\Omega_0)\right] \mathbf{a}^{\text{hem}}_{\text{bs,dif}}(\omega^*) \right\},$$

$$\mathbf{a}_{q,\lambda} = \frac{1 - \omega^* \mathbf{pa}}{1 - \omega(\lambda)\mathbf{pa}} \frac{1 - \omega(\lambda)}{1 - \omega^*} \mathbf{a}^q(\omega^*) \, .$$

Here $f_{\text{dir},\lambda}$ is the ratio of direct radiation to the total (direct and diffuse) radiation incident on the canopy; the coefficients $\mathbf{pt}_{\text{bs,dir}}$, $\mathbf{pt}_{\text{bs,dif}}$, $\mathbf{pt}_q$, $\mathbf{pa}$, and ω^* are evaluated from (49), (50), and (51); $\mathbf{t}^{\text{hem}}_{\text{bs,dir}}$, $\mathbf{t}^{\text{hem}}_{\text{bs,dif}}$, $\mathbf{a}^{\text{hem}}_{\text{bs,dir}}$, and $\mathbf{a}^{\text{hem}}_{\text{bs,dif}}$ are canopy transmittances and absorptances for the "black soil" problem at the reference leaf albedo ω^* which result from direct (subscript "bs,dir") and diffuse (subscript "bs,dif") incoming irradiance; $\mathbf{t}^q$ and $\mathbf{a}^q$ are the canopy transmittance and absorptance for the "S problem" at the reference leaf albedo ω^*. All these biome-dependent variables are stored in the CART file. An actual value of $f_{\text{dir},\lambda}$, which the MISR instrument provides together with BHR, is used to execute the first comparison test. For the second test, $f_{\text{dir},\lambda}=1$ is set; that is, the retrieved spectral BRF is used in this case. The FPAR is specified as described in section 9.

11. Conclusions

The following features of the LAI/FPAR retrieval technique are incorporated in the proposed MISR algorithm:

1. The measure theory allows us to build a function that relates canopy reflectances to parameters influencing the canopy reflectances without requiring a particular canopy radiation model. This parameter distribution function possesses the same properties as the cumulative distribution function used in probability theory. Thus a desired value of LAI can be expressed in the form of a mathematical expectation, hence its simplicity and the ability to account for uncertainties in input information.

2. Definition of the solution of the inverse problem does not depend on a particular canopy radiation model.

3. The contents of the CART file are precisely defined. Its elements are components of various forms of the energy conservation law. They are determined from general properties of radiative transfer and are independent of the models used to generate the CART.

4. The parameter distribution function is composed using elements of the CART file, and so the LAI retrieval algorithm does not depend on a particular canopy radiation model.

5. The precise definition of the CART file allows the formulation of requirements of the canopy radiation models used to generate the CART file.

6. Simple relationships between spectral properties of phytoelements and canopy absorptance and transmittance allow us to establish a simple relationship between retrieved LAI and FPAR. These relationships are also derived from the energy conservation law and do not depend on a particular canopy radiation model.

7. The simplicity of the LAI/FPAR retrieval algorithm, however, was reached at the expense of some complications in generating the CART file. Some of its elements are solutions of various ill-posed problems, and so a special technique was developed to generate the CART file.

Appendix

The measure theory is used to establish a relationship between measured reflectances and canopy structure. This

technique is a powerful way to relate values one quantifies (e.g., probabilities, weights, mass, volume, area, etc.) to the information one measures. Directly or indirectly, most modern approaches use measures. Therefore we use this technique to make the algorithm flexible. Unfortunately, some basic knowledge of the mathematical foundation of the modern probability theory [*Kolmogorov*, 1950] is required to follow sections 2 and 3. In our paper, we follow the original monograph of *Kolmogorov* [1950]. This theory can also be found in the work of [*Eisen*, 1969]. Standard measure theory is included mostly in programs for professional mathematicians only. Therefore nonmathematical communities may not be familiar with this theory. Chapter IX, sections 2-4 (pp. 337-348) of *Barnsley's* [1993] monograph is a good introduction to measures. Both measure and probability theories start with a description of spaces [*Barnsley*, section II.1, definition 1.1]. We introduce the following spaces:

1. Space of canopy realizations P. This space is represented by canopy structural types of global vegetation (biome), each representing patterns of the architecture of an individual tree and the entire canopy, and spectral properties of phytoelements ω_i at MISR bands λ_i, i=1,2,3,4 (section 5.5). Each biome is characterized by ground cover g, mean LAI of an individual tree L, and pattern of effective ground reflectances (ρ_1, ρ_2, ρ_3, ρ_4) in the MISR bands. A detailed parameterization of this space is discussed by *Knyazikhin et al.* [this issue]. The element p of this space is the vector p=(bio, ω_1, ω_2, ω_3, ω_4, ρ_1, ρ_2, ρ_3, ρ_4, L, g). Here bio can take six values only; one pattern (ω_1, ω_2, ω_3, ω_4) of the spectral leaf albedo per biome. Ground cover, the LAI of individual vegetation, and effective ground reflectance can vary within given biome-dependent ranges. Thus the space of canopy realization is supposed to represent patterns of existing vegetation canopies. The space P is the sum of six biome-dependent subset P_{bio}, bio=1, 2, ... , 6. The element of P_{bio} is the vector (ρ_1, ρ_2, ρ_3, ρ_4, L, g). The probability theory treats the spaces P and P_{bio} as sets of elementary events.

2. Spaces of observations of canopy reflectances D_A and D_r are introduced in (3). The probability theory treats the spaces D_A and D_r as sets of elementary events.

The measure theory requires the introduction of a sigma-field [*Barnsley*, section IX.2, definitions 2.1 and 2.3]. The Borel fields $B(P_{\text{bio}})$, $B(D_A)$, and $B(D_r)$ associated with P_{bio}, D_A, and D_r, respectively, are taken as the required sigma-fields in our paper [*Barnsley*, section IX.2, definition 2.5]. Elements of $B(P_{\text{bio}})$, $B(D_A)$, and $B(D_r)$ are defined to be events in probability theory. Note that $B(P_{\text{bio}})$, $B(D_A)$, and $B(D_r)$ are sets whose elements are subsets of P_{bio}, D_A, and D_r, respectively.

In order to relate LAI to the spaces P_{bio}, D_A, and D_r, we consider the functions $l(p)= gL$, $\bar{r}(\Omega_0,p)$, and $\vec{A}^{\text{hem}}(\Omega_0,p)$ which to every element p from P_{bio} set in correspondence, a value of LAI, a BRF-matrix (1), and the BHR-vector (2). These functions are supposed to be measured with respect to the Borel fields $B(P_{\text{bio}})$; that is,

$$S(L) = \{p \in P_{\text{bio}} \mid l(p) < L\} \in B(P_{\text{bio}}) \ ,$$

$$W_A(O_A; P_{\text{bio}}) = \{p \in P_{\text{bio}} \mid \vec{A}^{\text{hem}}(\Omega_0, p) \in O_A\} \in B(P_{\text{bio}}) \ ,$$

$$W_r(O_r; P_{\text{bio}}) = \{p \in P_{\text{bio}} \mid \bar{r}(\Omega_0, p) \in O_r\} \in B(P_{\text{bio}}) \ ,$$

where O_A and O_r (see (4)) are elements from $B(D_A)$ and $B(D_r)$, respectively. As mentioned above, $S(L)$, $W_A(O_A;P_{\text{bio}})$, and $W_r(O_r;P_{\text{bio}})$ are events in probability theory. For example, $S(L)$ is the event

$$\text{"value of LAI is less then } L\text{" ,} \tag{A1}$$

the subset $W_A(O_A;P_{\text{bio}})$ is the event,

"modeled BHRs belong to the intervals

$$[\tilde{A}_{\lambda_i}^{\text{hem}}(\Omega_0) - \varepsilon_i, \tilde{A}_{\lambda_i}^{\text{hem}}(\Omega_0) + \varepsilon_i] \, , \, i\text{=1,2,3,4" ,} \tag{A2}$$

where $\tilde{a}_\lambda^{\text{hem}}(\Omega_0)$ is the retrieved BHR at MISR spectral band λ, and ε_i is uncertainty in the BHR retrieval. The set $Q_A(L,O_A;P_{\text{bio}})$ introduced in section 2 is the product of the events $S(L)$ and $W_A(O_A;P_{\text{bio}})$; that is, $Q_A(L,O_A;P_{\text{bio}})$= $S(L) \cap W_A(O_A;P_{\text{bio}})$.

The steps done above are standard preparatory work to establish relationships between LAI and canopy reflectances under minimum conceptual assumptions. This technique leads to a diversity of relationships. For example, the curve [$l(p)$, $A_\lambda^{\text{hem}}(\Omega_0, p)$], where parameter p runs over the set P_{bio}, outlines biome-specific relationships between LAI and canopy reflectance $A_\lambda^{\text{hem}}(\Omega_0)$. This example demonstrates a widely used technique to derive and quantify various relationships, e.g., one plots all points [$l(p)$, $A_\lambda^{\text{hem}}(\Omega_0, p)$] on LAI-BHR, plane, and then evaluates a mean curve together with its dispersion. This mean curve quantifies a desired LAI-BHR relationship, while the dispersion characterizes its reliability. One can also, for example, rearrange elements in the sets P_{bio}, D_A, and D_r by ranking them in increasing order of the function $l(p)$. This involves a reparameterization of these sets in terms of LAI values (it will be recalled that LAI=$l(p)$) and separates elements (which are subsets!) from $B(P_{\text{bio}})$, $B(D_A)$, and $B(D_r)$ of different "sizes" with respect to the values of LAI; and this is the mathematical basis for quantifying the "size" of these elements with respect to the LAI values in terms of "weight," or "mass," or "volume," or "probability," etc. A successful way to assign different nonnegative real values to the elements of different "sizes" was realized in the notion of "measure" and Lebesgue's integral [*Lebesgue*, 1902]. This concept underlies modern probability theory and integration techniques.

Definition of a measure can be found in the work of [*Barnsley*, section IX.3, definition 3.1, p. 341]. The theory defines the probability of an event as a normalized measure; that is, it includes one more condition in the definition of the measure, namely, $\mu(X)$=1. In our paper, we weighted LAI values with respect to canopy reflectances by (8), (9) and (10). However, to justify this approach, it must be shown that the limits in (9) and (10) do not depend on the particular choice of the subdivision (8). The proof of this assertion is provided by a theorem [*Barnsley*, section IX.4, theorem 4.3, p. 347].

Really, let A be an arbitrary element from the sigma-field $B(P_{\text{bio}})$. We consider the characteristic function $\chi_A(p)$ whose values is 1, if $p \in A$, and zero otherwise. The subdivision (8) is a partition of P_{bio} [*Barnsley*, section IX.4, definition 4.3]. We consider a function $\chi_A^N(p)$ defined as

$$\chi_A^N(p) = \sum_{k=1}^{N} \chi_A(p_k) \chi_{P_{\text{bio},k}}(p) \equiv \sum_{k=1}^{N} \chi_{A \cap P_{\text{bio},k}}(p) \ , \quad (A3)$$

where $p_k \in P_{\text{bio},k}$ is a point from the set $P_{\text{bio},k}$. Let us introduce a measure of the set A as the mean of $\chi_A^N(p)$ over partition (8) and points p_k; that is,

$$\mu^N[A] = \frac{1}{N} \sum_{k=1}^{N} \chi_A^N(p_k) \ .$$

The value $\mu^N[A]$ satisfies the definition of measure [*Barnsley*, section IX.3, definition 3.1, p. 341]. Moreover, it follows from (A3) and (8) that $\mu^N[P_{\text{bio}}] = 1$. It means $\mu^N[A]$ is the probability of the event $A \in B(P_{\text{bio}})$. This value depends on the partition (8), N and the choice of the points p_k. However, the theorem [*Barnsley*, section IX.4, theorem 4.3, p. 347] asserts that (1) the function (A3) converges uniformly to $\chi_A(p)$ when the diameter of partition tends to zero; (2) the sequence $\mu^N[A]$ converges to a value $\mu[A]$; and (3) the value of the limit is independent of the particular sequence of partitions and of the choices of $p_k \in P_{\text{bio},k}$. Thus the measure defined as

$$\mu[A] = \lim_{N \to \infty} \mu^N[A] \qquad (A4)$$

does not depend on subdivision (8).

Let us consider how (A4) is related to the LAI distribution functions $F_{A,\text{bio}}$ and $F_{r,A,\text{bio}}$ introduced in (9) and (10). The function $F_{A,\text{bio}}$ is the probability of the event $S(L)$ (equation (A1)) under the condition that the event $W_A(O_A; P_{\text{bio}})$ (equation (A2)) already occurred. It follows from the definition of the conditional probability that

$$F_{A,\text{bio}}(L) = \frac{\mu[S(L) \cap W_A(O_A; P_{\text{bio}})]}{\mu[W_A(O_A; P_{\text{bio}})]} \ .$$

In section 2, this definition is presented in an equivalent form, namely,

$$\begin{aligned} F_{A,\text{bio}}(L) &= \lim_{N \to \infty} \frac{\mu^N[S(L) \cap W_A(O_A; P_{\text{bio}})]}{\mu^N[W_A(O_A; P_{\text{bio}})]} \\ &= \lim_{N \to \infty} \frac{\mu^N[Q_A(L, O_A; P_{\text{bio}})]}{\mu^N[Q_A(\text{LAI}_{\max}, O_A; P_{\text{bio}})]} \ . \end{aligned}$$

If the events $W_A(O_A; P_{\text{bio}})$ and $S(L)$ are independent, then $F_{A,\text{bio}}(L) = \mu[S(L)]$. This underlies our definition of the saturation domain (18): a measured spectral BHR belongs to the saturation domain if the events $W_A(O_A; P_{\text{bio}})$ and "value of LAI is greater or equal to L^*" are independent. The function $F_{r,A,\text{bio}}$ is the probability of the event $S(L)$ under the condition that the event $W_r(O_r; P_{\text{bio}}) \cap W_A(O_A; P_{\text{bio}})$ already occurred.

We also note one interesting property of the functions $F_{A,\text{bio}}$ and $F_{r,A,\text{bio}}$. It follows from the definition of $F_{A,\text{bio}}$ that if there exists only one parameter $p^* \in P_{\text{bio}}$ for which modeled BHRs belong to the intervals (A2), then the function $F_{A,\text{bio}}$ coincides with the Heaviside function; that is,

$$F_{A,\text{bio}}(L) = \begin{cases} 0, & \text{if } L \le L^*, \\ 1, & \text{otherwise} \end{cases}$$

where $L^* = l(p^*)$. It means that the solution of the inverse problem defined by (11) coincides with this unique solution $L^* = l(p^*)$. The same is true if there are many parameters $p \in P_{\text{bio}}$ for which modeled BHRs belong to the intervals (A2), while values $l(p)$ slightly vary about a value L^*. It means that if the inverse problem has a unique solution, the algorithm specifies it. If not, the algorithm provides the most probable solution.

References

Barnsley, M. F., *Fractals Everywhere*, 531 pp., Academic, San Diego, Calif., 1993.

Bass, L.P., A.M.Volocsvhenko, and T.A.Germogenova, *Methods of Discrete Ordinates in Radiation Transport Problems* (in Russian, with English abstract), 231 pp., Inst. Appl. Math., Russ. Acad. of Sci., Moscow, 1986.

Diner, D.J., J.V.Martonchik, C. Borel, S.A.W. Gerstl, H.R. Gordon, Y. Knyazikhin, R. Myneni, B. Pinty, and M.M. Verstraete, MISR: Level 2 surface retrieval algorithm theoretical basis, *JPL Internal Doc. D-11401, Rev. C*, Calif. Inst. of Technol., Jet Propul. Lab., Pasadena, 1998a.

Diner, D.J., W.A. Abdou, H.R. Gordon, R.A. Kahn, Y. Knyazikhin, J.V.Martonchik, S. McMuldroch, R.B. Myneni, and R.A. West, Level 2 ancillary products and data sets algorithm theoretical basis, *JPL Internal Doc. D-13402, Rev. A*, Calif. Inst. of Technol., Jet Propul. Lab., Pasadena, 1998b.

Eisen, M., *Introduction to Mathematical Probability Theory*, 535 pp., Prentice Hall, Englewood Cliffs, New Jersey, 1969.

Germogenova, T.A., *The Local Properties of the Solution of the Transport Equation* (in Russian), 272 pp., Nauka, Moscow, 1986.

Jacquemoud, S., F. Barret, and J.F. Hanocq, Modeling spectral and bidirectional soil reflectance, *Remote Sens. Environ., 41*, 123-132, 1992.

Knyazikhin, Y., G. Mießen, O. Panfyorov, and G. Gravenhorst, Small-scale study of three-dimensional distribution of photosynthetically active radiation in a forest, *Agric. For. Meteorol., 88*, 215-239, 1997.

Knyazikhin, Y., J.V., Martonchik, R.B. Myneni, D.J. Diner, and S.W. Running, Synergistic algorithm for estimating vegetation canopy leaf area index and fraction of absorbed photosynthetically active radiation from MODIS and MISR data, *J. Geophys. Res.*, this issue.

Kolmogorov, A.M., *Foundations of the Theory of Probability*, 71 pp., Chelsea, New York, 1950.

Kranigk, J., *Ein Model für den Strahlungstransport in Fichtenbeständen*, 127 pp., Cuvillier, Göttingen, Germany, 1996.

Kuusk, A., The hot spot effect of a uniform vegetative cover, *Sov. J. Remote. Sens., 3*, 645-658, 1985.

Lebesgue, H., Intégrale, Longueur, Aire, *Thése (Paris 1902) ou Annali Mat Pura e Appl.*, vol. 3, Nr. 7, 231-359, 1902.

Li, X., and A.H. Strahler, Geometrical-optical bidirectional reflectance modeling of the discrete crown vegetation canopy:

Effect of crown shape and mutual shadowing, *IEEE Trans. Geosci. Remote Sens.*, *30*, 276-292, 1992.

Marshak, A., Effect of the hot spot on the transport equation in plant canopies, *J. Quant. Spectrosc. Radiat. Transfer, 42,* 615-630, 1989.

Martonchik, J.V., D.J. Diner, B. Pinty, M.M. Verstraete, R.B. Myneni, Y. Knyazikhin, and H.R. Gordon, Determination of land and ocean reflective, radiative and biophysical properties using multi-angle imaging, *IEEE Trans. Geosci. Remote Sens.*, *36*, 1266-1281, 1998.

Myneni, R.B., Modeling radiative transfer and photosynthesis in three-dimensional vegetation canopies, *Agric. For. Meteorol.*, *55*, 323-344, 1991.

Myneni,R.B., S. Maggion, J. Iaquinta, J.L.Privette, N. Gobron, B. Pinty, D.S. Kimes, M.M. Verstraete, and D.L. Williams, Optical remote sensing of vegetation: Modeling, caveats and algorithm, *Remote Sens. Environ*, *51*, 169-188, 1995.

Myneni, R.B., R.R. Nemani, and S.W. Running, Estimation of global leaf area index and absorbed PAR using radiative transfer model, *IEEE Trans. Geosci. Remote Sens.*, *35*, 1380-1393, 1997.

Pinty, B., and M.M. Verstraete, Modeling the scattering of light by vegetation in optical remote sensing, *J. Atmos. Sci.*, *55*, 137-150, 1998.

Pinty, B., M.M.Verstraete, and R.E.Dickenson, A physical model for predicting bidirectional reflectance over bare soils, *Remote Sens. Environ., 27*, 273-288, 1989.

Pokrowski, G.I., Über die Helligkeitsverteilung am Himmel (in German), *Phys. Z.*, *30*, 697-700, 1929.

Ross, J., *The Radiation Regime and Architecture of Plant Stands*, 391 pp., Dr. W. Junk, Norwell, Mass., 1981.

Ross, J., and T. Nilson, A mathematical model of radiation regime of plant cover, in *Actinometry and Atmospheric Optics* (in Russian), Valgus, Tallin, Estonia, 1968.

Ross, J., Y. Knyazikhin, A. Kuusk, A. Marshak, and T. Nilson, *Mathematical Modeling of the Solar Radiation Transfer in Plant Canopies* (in Russian, with English abstract), 195 pp., Gidrometeoizdat, St. Peterburg, Russia, 1992.

Running, S.W., R.B. Myneni, R. Nemani, J. Glassy, MOD15 LAI/FPAR algorithm theoretical basis document. MODIS LAI (leaf area index) and MODIS FPAR (fraction of absorbed photosynthetically active radiation), *Tech. Rep.*, Sch. of For., Univ. of Mont., Missoula, 1996.

Tikhonov, A.N., and V. Y. Arsenin, *Methods for Solving Ill-Posed Problems* (in Russian), 288 pp., Nauka, Moscow, 1986.

Vladimirov, V.S., Mathematical problems in the one-velocity theory of particle transport, *Tech. Rep. AECL-1661*, At. Energy of Can. Ltd., Chalk River, Ontario, 1963.

D.J. Diner and J.V. Martonchick, Mail Stop 169-237, Jet Propulsion Laboratory, California Institute of Technology, 4800 Oak Grove Drive, Pasadena, CA 91109. (e-mail: djd@jord.jpl.nasa.gov; jvm@ jord.jpl.nasa.gov)

N. Gorbon, B. Pinty, and M. Verstraete, Space Application Institute of the EC Joint Research Center, TP 440, I-21020 Ispra (VA), Italy. (e-mail: nadine.gobron@jrc.it; bernard.pinty@irc.it; michel.verstraete@jrc.it)

Y. Knyazikhin and R.B. Myneni, Dep. of Geography, Boston University, 675 Commonwealth Avenue, Boston, MA 022150. (e-mail: jknjazi@crsa.bu.edu; rmyneni@crsa.bu.edu)